Surface & Coatings Technology 394 (2020) 125878

Contents lists available at ScienceDirect

Surface & Coatings Technology

journal homepage: www.elsevier.com/locate/surfcoat

The interaction between the osteosarcoma cell and stainless steel surface, modified by high-fluence, nanosecond laser pulses

Matej Hočevar[a], Barbara Šetina Batič[a], Matjaž Godec[a], Veno Kononenko[b], Damjana Drobne[b], Peter Gregorčič[a,c,*]

[a] Institute of Metals and Technology, Lepi pot 11, 1000 Ljubljana, Slovenia
[b] Department of Biology, Biotechnical Faculty, University of Ljubljana, Večna pot 111, 1000 Ljubljana, Slovenia
[c] Faculty of Mechanical Engineering, University of Ljubljana, Aškerčeva 6, 1000 Ljubljana, Slovenia

ARTICLE INFO

Keywords:
Laser surface engineering
Nanosecond-laser ablation
Laser texturing
MG63 cells
Cell adhesion

ABSTRACT

The irradiation of metallic surfaces by high-fluence laser pulses in an oxygen-containing atmosphere inevitably modifies the surface topography, chemistry, and wettability. These modifications significantly influence cell-surface interactions and, consequently, surface biocompatibility. We investigate how surface texturing by high-fluence nanosecond laser pulses from a Nd:YAG laser (wavelength of 1064 nm) influences cell adhesion and morphology with the aim of assessing its impact on initial cell behaviour. Quantitative and qualitative analysis of osteosarcoma cell adhesion, viability, and cell morphology were evaluated after 24-hour exposure to non-treated and laser-textured stainless-steel (AISI 316L) surfaces by fluorescent and scanning electron microscopy. The results reveal that this, initial interaction between the cells and the laser-textured surfaces leads to round shaped cells with a smaller footprint. Contrarily, on the non-processed stainless-steel and control-glass surfaces the polygonal, highly elongated, and flattened cells are observed. The cells on the laser-textured surfaces are less dendritic, with short tubular protrusions and an overexpression of extracellular vesicles, which are rarely found on non-treated and control samples. This likely happens due to the formation of nanostructured, high-temperature oxides that are induced by laser ablation. The analysis by X-ray photoelectron spectroscopy reveals that the laser-textured stainless-steel surfaces contain Cr hexavalent oxide, which is more toxic than the native oxide layer on the non-processed samples.

1. Introduction

In the last decade, considerable effort has been devoted to engineering the surfaces of biomaterials in order to improve their biocompatibility without altering the properties of the bulk material. The ability of biological systems to respond to topographical features or chemical stimuli has led to the development of next-generation, innovative materials for a wide variety of applications. In-vitro studies have confirmed that nanotopographical modifications may regulate cellular behaviour and function [1,2]. Metallic materials, such as stainless steel, are widely used in medicine due to their good combination of mechanical properties, durability, and low-cost fabrication in comparison with polymeric or ceramic biocompatible materials. However, they often exhibit limited biocompatibility and a lack of biofunctionalities for certain applications [3–6]. Most of these limitations could be reduced by changing the material surface properties in terms of surface morphology, topography, chemistry, and (as a result of both), wettability [4,7,8].

A number of surface treatment methods, such as machining, lithography, plasma surface treatment, ion beam processing, and surface coatings, have been developed to optimize and control material surface-cell interactions [9,10]. By affecting the wettability characteristics through morphological and chemical modifications, these methods enable manipulation of biological-cell response to particular materials [4,7,11–13]. It is known from the literature that surface features, including surface roughness and topography, surface chemistry, and surface wettability, represent an important regulator of protein adsorption, cell adhesion, cell spreading, cell migration, and differentiation either via the enhanced formation of focal contacts, the distribution of focal contacts, or through the selective adsorption of proteins required for cell attachment [1,4,7,14,15].

Recently, laser surface engineering [16], in which laser pulses are used for flexible surface modifications at the micro- and nanoscale, has proven to be an efficient, robust, affordable, and chemicals-free

* Corresponding author at: Faculty of Mechanical Engineering, University of Ljubljana, Aškerčeva 6, 1000 Ljubljana, Slovenia.
E-mail address: peter.gregorcic@fs.uni-lj.si (P. Gregorčič).

https://doi.org/10.1016/j.surfcoat.2020.125878
Received 5 March 2020; Received in revised form 30 April 2020; Accepted 4 May 2020
Available online 06 May 2020

Table 1
Chemical composition of investigated AISI 316L stainless steel in wt%.

Material	Fe	Cr	Ni	Mo	Mn	Si	Cu	P	C	S	V	N
	Balance	16.9	10.04	2.07	1.84	0.57	0.41	0.036	0.019	0.0009	0.077	0.044

approach for surface modification and functionalization [11,17–22]. Laser surface processing has many advantages over other surface modification techniques due to its flexibility, simplicity, controllability, and ability to produce various micro- and nanostructures that are suitable for different applications [7,11,23,24]. Surfaces that mimic the natural environment of cells are crucial for controlling cell adhesion, proliferation, differentiation, and regeneration [4]. Solutions for technical problems related to material surfaces are often inspired by hierarchical surfaces in nature [20]: lotus leaves (wettability) [19,25–27], shark skin (antifouling) [28], gecko feet (adhesion) [29], and bone (functional light-weight structures with outstanding mechanical properties) [4]. Mimicking these surfaces is possible through the utilization of laser surface micro- and nanostructuring [19,25,28]. Laser surface engineering presents an excellent alternative to other technologies due to the ability to exert precise control over the morphology and wettability of the modified surface and to process different surfaces and account for changing surface properties (including surface chemistry [17,30,31]) without affecting the properties of the bulk material [7,23,24]. As a result, laser surface engineering has attracted considerable attention in recent years within the field of biomaterials.

Several research groups have studied cell behaviour on laser-textured surfaces, mainly using ultra short (femtosecond and picosecond) laser pulses, with very promising results. They observed that material surfaces with controlled micro- and nanotopographical features can influence cell adhesion (e.g., increase or decrease attachment) [24,32,33], proliferation [34–36] and differentiation [34], and affect overall cell behaviour, such as orientation, migration, and cell morphology [33,37]. Moreover, it has been also proven that laser surface texturing may promote antibacterial properties resulted from reduced bacterial adhesion and bactericidal effect [38–41].

Ultrashort laser systems present state-of-the-art approach for surface texturing despite some disadvantages, such as high cost [18]. However, comparably good results, in terms of improved corrosion resistance [42], surface wettability control [8,17,31,43–47], and the production of various micro- and nanotopographies [22,48], have recently been achieved by less expensive nanosecond laser systems [49,50]. In order to assure the wide application of this technology, research on the cell interactions with nanosecond laser-textured surfaces is still needed.

One of the most studied aspects of surface engineered biomaterials has to do with its biomedical applications, particularly with regards to osteoblast adhesion. Upon contact with the material, the surface influences cell proliferation and differentiation, which is manifested in the cell's capacity to attach and spread [15]. The cyto-compatibility of a material can be assessed in vitro by observing the viability and adhesion of cells at the substratum interface. Adherent cells are complex, self-sustaining units that require an extracellular matrix for anchorage in order to proliferate and undergo differentiation [1]. In adherent cells, a network of dynamic contractile machinery facilitates both cellular motility and the formation of protrusions termed ‘lamellipodia’ - structures essential for cellular spreading and polarisation. Lamellipodia are associated with fine, hair-like protrusions termed ‘filopodia’, which contain a core of extended actin filament bundles and actively probe the external environment to gather spatial, topographical, and chemical information [1,51]. Exosome formation provides a characterization of a cell's communication with other cells and its surroundings [52]. Exosomes are 30–100 nm extracellular membrane-bound vesicles of endocytic origin. Exosomal secretion functions as a mediator of cell-to-cell communication, which means that exosomes play a crucial role in both physiological and pathological processes. Saeed-Zidane et al. [53] provided evidence that cells exposed to oxidative stress conditions respond by activating cascades of cellular antioxidant molecules which can also be released into the extracellular environment through exosomes. Moreover, their generation can be induced by many factors including extracellular stimuli, such as microbial attack and other stress conditions. The primary role attributed to exosomes is the removal of unnecessary proteins from cells.

In this study, we perform nanosecond-laser texturing of stainless-steel surfaces and assess in detail the resulting morphology, chemistry, wettability, and adhesion of human osteoblast-like osteosarcoma cells (MG63). By doing this, we examine the correlation between laser-induced surface modifications (on micro-, nano- and molecular- levels) and the initial cell behaviour in terms of cell adhesion pattern, morphology and the presence of exosome biogenesis as an indicator of cellular stress.

2. Materials and methods

2.1. Materials

Samples (diameter of 10 mm and thickness of 1.5 mm) were made from commercially available AISI 316L stainless steel sheets with a 2B surface finish, which are produced by cold-rolling, annealing, pickling, and light passage through highly polished rolls. The chemical composition (Table 1) of the material used was assessed by an X-ray fluorescence (XRF) spectrometer (Thermo Scientific Niton XL3t GOLDD+), Carbon/Sulfur analyzer (ELTRA CS-800), and ICPS-OES (Agilent 720).

2.2. Laser texturing

Stainless-steel 316L samples with a 2B surface finish (as received, non-polished) were ultrasonically cleaned in absolute ethanol for 12 min and further processed in an open-air atmosphere by direct laser texturing at fluences significantly higher than the threshold fluence for laser ablation. This was done by using a marking nanosecond Nd:YAG pulsed laser with a wavelength of 1064 nm and pulse duration of 95 ns (full width at half maximum). We used a pulse repetition rate of 1 kHz at an average power of 0.6 W. Thus, the pulse energy equalled 0.6 mJ and, considering the beam waist diameter of 0.05 mm, resulted in the peak fluence of 61 J cm^{-2}. The threshold fluence for ablation of the material used equals 3.8 J cm^{-2} [46]. The surface was processed by leading the laser beam over the parallel lines with scanning velocity $v = 1.6$ mm s^{-1} (resulting in a spot separation of $\Delta x = 1.6$ µm and overlapping adjacent pulses of 97%), while the lines were separated by $\Delta y = 50$ µm. After laser texturing the surfaces were put into plastic boxes and were stored in atmospheric air.

2.3. Surface characterization

The surfaces were characterized in terms of surface morphology, topography, roughness, chemistry, and wettability:

- *Surface morphology*, *topography*, *and roughness* of the non-treated and laser-textured 316L samples were examined with a field emission scanning electron microscope (SEM, JEOL JSM-6500F) and the optical 3D surface measuring system InfiniteFocus (IFM, Alicona), using IF-MeasureSuite® 5.1 software. SEM was employed for detailed visual analysis of micro and nanoscale surface features, while IFM was used for quantitative assessment of the surface topography.

This includes the following 3D surface roughness parameters: arithmetical mean height (S_a); root mean square height (S_q); and maximum height (S_z).

- *The chemical composition and changes of surface chemistry* after laser texturing were examined by SEM coupled with an energy dispersive spectrometer (EDS, INCA X-SIGHT LN2 with INCA ENERGY 450 software) and X-ray photoelectron spectroscope (XPS, MICROLAB 310F VG-Scientific) using a monochromatic Al Kα X-ray source (1486.6 eV) operated at an accelerating voltage of 12.5 kV and emission current of 16 mA (200 W power). XPS measurements were processed by the Avantage® 3.41 data-acquisition & data-processing software program, while Casa XPS (http://www.casaxps.com) software was used for detailed processing.
- *The surface wettability* after laser texturing was analysed using a goniometer of our own design. The surface wettability was determined by apparent contact angle (APA), θ, measurements using distilled water droplets with a volume of 5 μL at room temperature. Images of the water droplet on the surface were captured using a CCD camera, and the APA was measured from the acquired images, as described in Ref. [46]. Due to the hydrophilic nature of the surfaces immediately after laser texturing [17], none of the tested surfaces had a roll-off angle.

2.4. Cell culture

Human bone osteosarcoma cells [MG-63; (ATCC® CRL-1427™)] were used for the adhesion behaviour assessment on non-treated 2B surface finished and laser-textured 316L samples. Cells were cultured under controlled conditions (37 °C, 5% CO_2, high humidity) in Dulbecco's modified Eagle's medium (DMEM), supplemented with 4 mM L-glutamine,10% (v/v) fetal bovine serum (FBS) and 1% Penicillin-Streptomycin solution (Sigma-Aldrich, Steinheim, Germany) and were routinely passaged twice a week. Prior to the experimental work, the cells were confirmed to be mycoplasma negative using the MycoAlert™ Kit (Lonza, Basel, Switzerland).

2.5. Cell adhesion and viability assay

Three sets of both non-treated and laser-textured 316L samples were UV sterilised and aseptically put into 12-well plates. Glass disks (diameter of 10 mm; Paul Marienfeld, Germany) with apparent contact angle of 20° ± 5° were used as a control group. A volume of 2.5 mL of trypsinized suspended MG63 cells (passages 11–15) in supplemented cell culture medium was plated at a seeding density of 2×10^4 cells cm^{-2} into each well, with each well containing one sample. After 24-hour incubation under controlled laboratory conditions (5% CO_2/95% air at 37 °C) to allow the cells to adhere, the samples with cells were rinsed with Dulbecco's Phosphate-Buffered Saline (to remove any floating, unattached cells) and stained with 2 μg/mL Hoechst 33342 and 2 μg/mL Propidium iodide for 20 min. Hoechst 33342 stains the nuclei of all cells blue, while Propidium iodide stains the nuclei of non-viable cells (cells with damaged plasmalemma) red.

Stained cells were observed with a fluorescent microscope (Axio Imager.Z1; Carl Zeiss, Jena, Germany) immediately after staining. At least 15 images per sample for each type of surface were randomly taken at 100× magnification, and each of the non-treated, laser-textured and glass surfaces was investigated in triplicate. Quantitative image analysis of the density of attached cells and cell viability were performed using the free software program ImageJ [54], where the number of viable attached cells (based on the number of blue nuclei) and the number of non-viable cells (based on the number of red nuclei) were evaluated. All results were normalized to the sample surface area.

The data from cell adhesion assay were expressed as arithmetic mean ± standard deviations (SD) and were statistically analysed using GraphPad Prism software (GraphPad Software, San Diego, CA) by the nonparametric two-tailed Mann-Whitney test. The p values lower than 0.05 were considered statistically significant.

2.6. Cell adhesion pattern and cell morphology analyses

After cell adhesion and cell viability observation, the samples with attached cells were further prepared for SEM examination. Samples with attached cells were submerged into Karnovsky fixative, composed of 2.5% glutaraldehyde (SPI Supplies, West Chester, PA, USA) and 0.4% paraformaldehyde (Merck KGaA, Darmstadt, Germany) in 1 M Na-phosphate buffer ($NaH_2PO_4 \cdot 2H_2O$ and $Na_2HPO_4 \cdot 2H_2O$; Merck KGaA, Darmstadt, Germany). After 3 h fixation at room temperature, the fixative was removed and samples were washed 3 × 10 min with 1 M Na-phosphate buffer. Post-fixation of the samples was done using 1% osmium tetroxide (OsO_4) (SPI Supplies, West Chester, PA, USA; 60 min), followed by washing in distilled water (3 × 10 min). Samples were dehydrated with 30% ethanol (EtOH; Merck KGaA, Darmstadt, Germany; 10 min), 50% EtOH (10 min), 70% EtOH (10 min), 80% EtOH (10 min), 90% EtOH (10 min), and absolute EtOH (10 min). Further dehydration steps were performed with a mixture of hexamethyldisiloxane (HMDS; SPI Supplies, West Chester, PA, USA) and absolute EtOH (1:2, v/v, 10 min; 1:1, v/v, 10 min) and with absolute HMDS (10 min), which was finally left to evaporate for 24 h. Samples were sputter-coated with gold using a Precision Etching Coating System (682 PECS, Gatan, Pleasanton, USA). SEM was used to visualize the attachment pattern and morphology of adhered MG63 cells on glass, non-treated and laser-textured stainless steel surfaces.

3. Results

3.1. Surface topography and morphology

As expected [17], SEM investigation reveals significant differences in surface morphology between the non-treated and laser-textured samples (Fig. 1). The non-treated sample exhibits a typical smooth, grain-structured-like morphology with a network of subsurface crevices between the grain boundaries. They are a result of the pickling treatment following the cold-rolling stage during the steel's production (Fig. 1a). Grain size ranges from 3 to 20 μm in diameter and the crevices between the grain boundaries are up to 1.5 μm deep. On the surface of the laser-textured sample, a hierarchical micro- and nanostructure is observed. In this case, 100-μm-deep micro-channels are separated by 50 μm and covered with a hierarchical structure of micro bumps (up to 10 μm) and a nanostructured surface (oxide layer) (Fig. 1b) that appears due to melting and oxidation caused by laser ablation (see also section S1 in Supplementary Material).

Furthermore, IFM 3D surface images with corresponding profiles (Fig. 1c and d) and topography measurements show that direct laser texturing increases both the area and roughness of the surfaces (S_a = 16.2 μm ± 0.55 μm) compared with the much smoother non-treated surfaces (S_a < 0.04 μm; Table 2). For example, laser texturing increases the surfaces of the laser-textured samples by 3.5-times (Table 2). Additional measurement details are explained in section S1 of Supplementary Material.

3.2. Surface chemistry

The thick oxide layer on the laser-textured sample is clearly visible in Fig. 2, where EDS analysis was conducted on a nanostructured micro bump with a partly removed layer (Fig. 2a), and compared with the non-treated sample (Fig. 2b). The EDS measurements clarify that on the laser-textured sample between points 3–9, the oxide layer was broken and the measured weight percentage of O within the selected points confirms that the base material after laser texturing is covered with a thick oxide layer (Fig. 2c). By contrast, the EDS measurements obtained from the non-treated sample shows much lower percentage of O within the selected points (Fig. 2c and Table S2). This clearly proves that laser

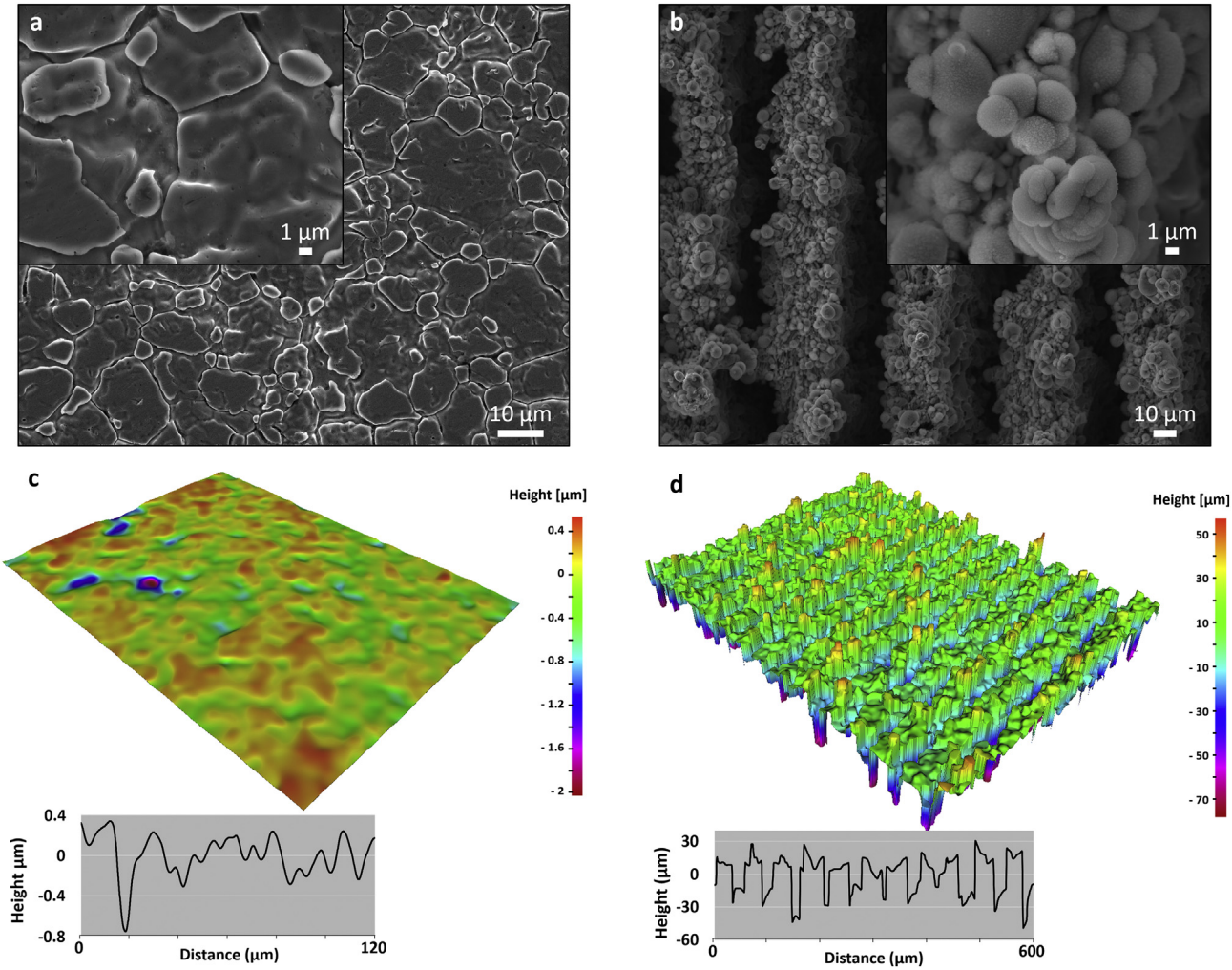

Fig. 1. SEM-revealed morphology of (a) non-treated and (b) laser-textured surfaces and 3D surface topography with corresponding topography profiles of (c) non-treated and (d) laser-textured samples.

texturing at high fluences results in significant surface oxidation of stainless steel compared with non-treated surfaces, where a thin oxide layer is uniformly present on the surface.

To understand the surface modifications at a molecular level, we further performed XPS measurements. Survey XPS spectra of laser treated and non-treated samples in the as-received state are shown in Fig. 3. The spectra have been adjusted to account for charging by setting the C 1s peak to energy typical for adventitious carbon at 284.8 eV. Table 3 gives the composition of the surface layers of both tested samples. The carbon content is significant in both cases due to surface contamination, but is approximately three times larger in the case of the laser-textured sample. This is probably due to the much larger surface area of the sample and thus the presence of more surface sites for carbon contamination. This difference is also highlighted in the spectra, where a significantly larger C (and also O) peak can be seen in the case of the laser-textured sample.

High-resolution spectra of Cr and Fe peaks confirm the presence of an oxide layer on both samples. The Fe 2p3/2 high-resolution spectra are shown in Fig. 4a and b. In this case, the peak has been fitted with five components, belonging to Fe metal, FeO, and Fe^{2+} and Fe^{3+} of Fe_3O_4 and Fe_2O_3, respectively, according to data found in the literature regarding peak positions, peak line shapes, and widths of individual components [55]. Fig. 4c and d shows the spectra of Cr 2p3/2 peaks and their deconvolutions. The spectra have been fitted with four major components, belonging to Cr(III) oxide (Cr_2O_3), Cr(VI) oxide (CrO_3), and $Cr(OH)_3$ hydroxide, as well as a metallic component. The parameters of the fitting have been modelled on data from the literature [56,57], with a single component for Cr_2O_3.

Cell viability can also be greatly impacted by the type of oxide layer that is present on the surface. For this reason, we used the deconvoluted

Table 2
Surface roughness parameter values.

Sample	S_a (µm)	S_q (µm)	S_z (µm)	Projected[a]/true[b] area ratio
316L non-treated	0.20 ± 0.01	0.28 ± 0.02	6.45 ± 2.51	1.004 ± 0.002
316L laser-textured	16.2 ± 0.6	20.8 ± 0.5	135 ± 4.2	3.57 ± 0.08

Values are given as mean ± standard deviation.
[a] Projected area is defined as an IFM scan area (defined by the magnification and size of the scanning area).
[b] True area is defined as the true measured surface, depending on the topography.

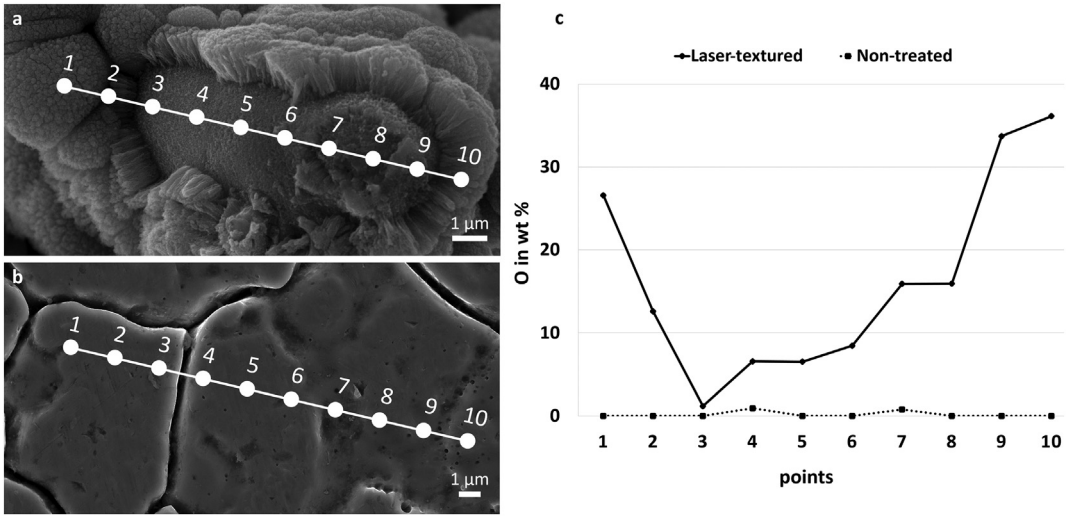

Fig. 2. SEM micrographs of (a) laser-textured and (b) non-treated surfaces with (c) corresponding EDS O element analyses.

high-resolution spectra to determine the amount of each Cr- and Fe-oxide present in the surface layer. The amount of different Cr-oxide and Fe-oxide components on the tested sample surfaces are shown in Fig. 5. These results reveal that no metal Cr or Fe is present on the surface of the laser-textured sample; rather, the laser-textured surface is composed of Fe^{3+}, Fe_2O_3, $Cr(OH)_3$, Cr_2O_3, and CrO_3.

Table 3
Surface composition of the as-received samples in atomic %.

Sample	O 1s	C 1s	Cr 2p	Fe 2p
316L non-treated	64	20	6	9
316L laser-textured	35	58	1	4

3.3. Surface wettability after laser texturing

Laser surface processing influenced the wetting behaviour of the stainless steel. While the contact angle measurements reveals that the non-treated 316 L sample exhibited slightly hydrophobic behaviour ($\theta = 95.0^\circ \pm 6.4^\circ$), the contact angle of a base material (i.e., the Young contact angle) can only be measured on an ideal flat surface [58,59]. Therefore, we highly polished ($R_a = 25 \pm 2$ nm) one of the non-processed 316 L samples and measured the Young contact angle to be $\theta_Y = 81.6^\circ \pm 5.7^\circ$. On the other hand, immediately after laser-texturing, the water droplet spreads over the whole textured surface and forms a thin film (see also Ref. [17]). Thus, the surface after texturing is superhydrophilic in a saturated Wenzel regime with contact angle $\theta = 0^\circ$ [58,60,61].

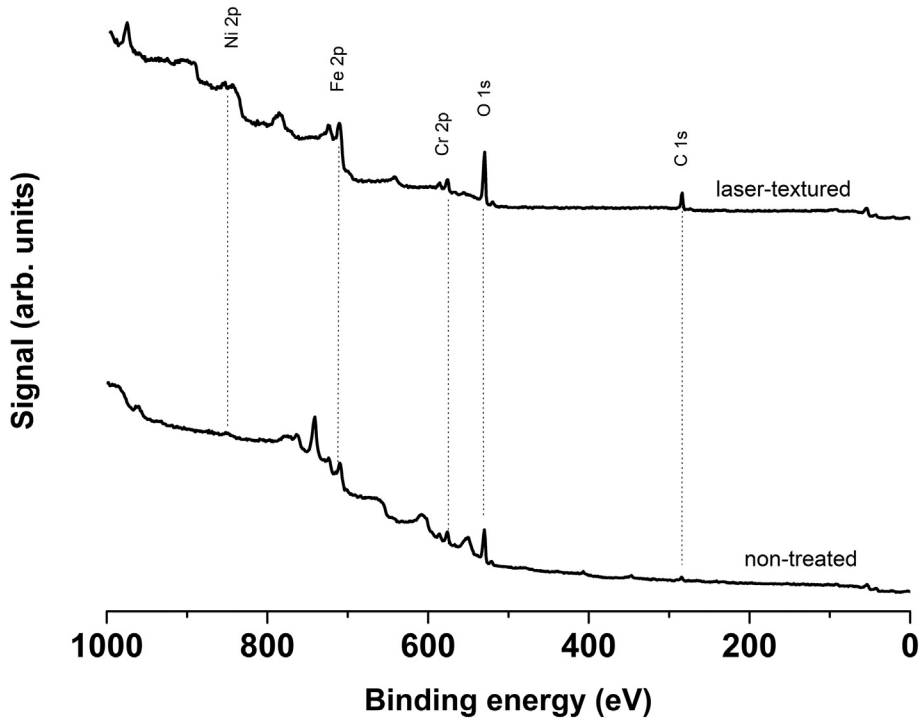

Fig. 3. Survey XPS spectra of laser-textured and non-treated (polished) samples, in the as-received state.

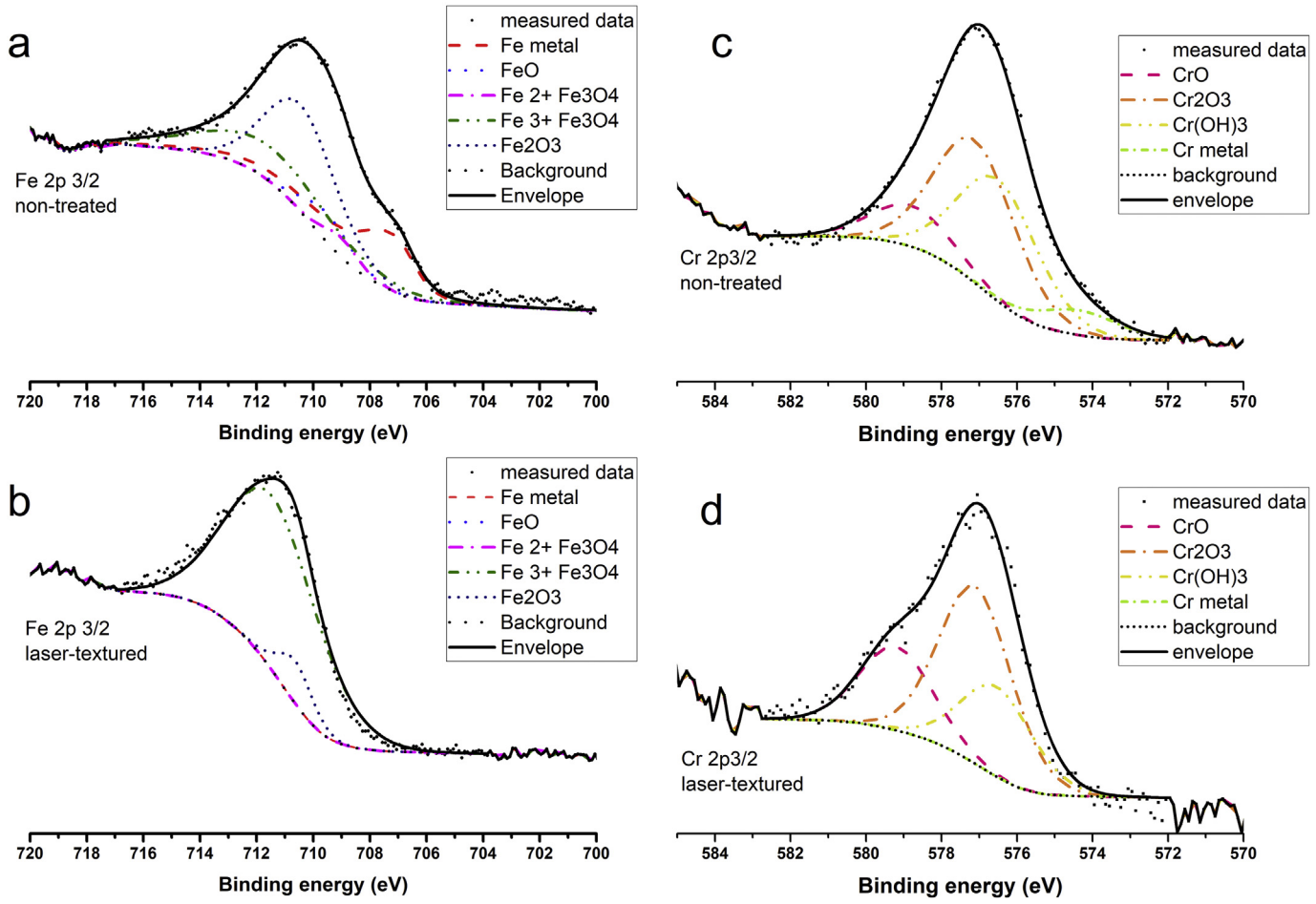

Fig. 4. High-resolution XPS spectra of Fe for (a) as-received and (b) laser-textured samples and of Cr for (c) as-received and (d) laser-textured samples.

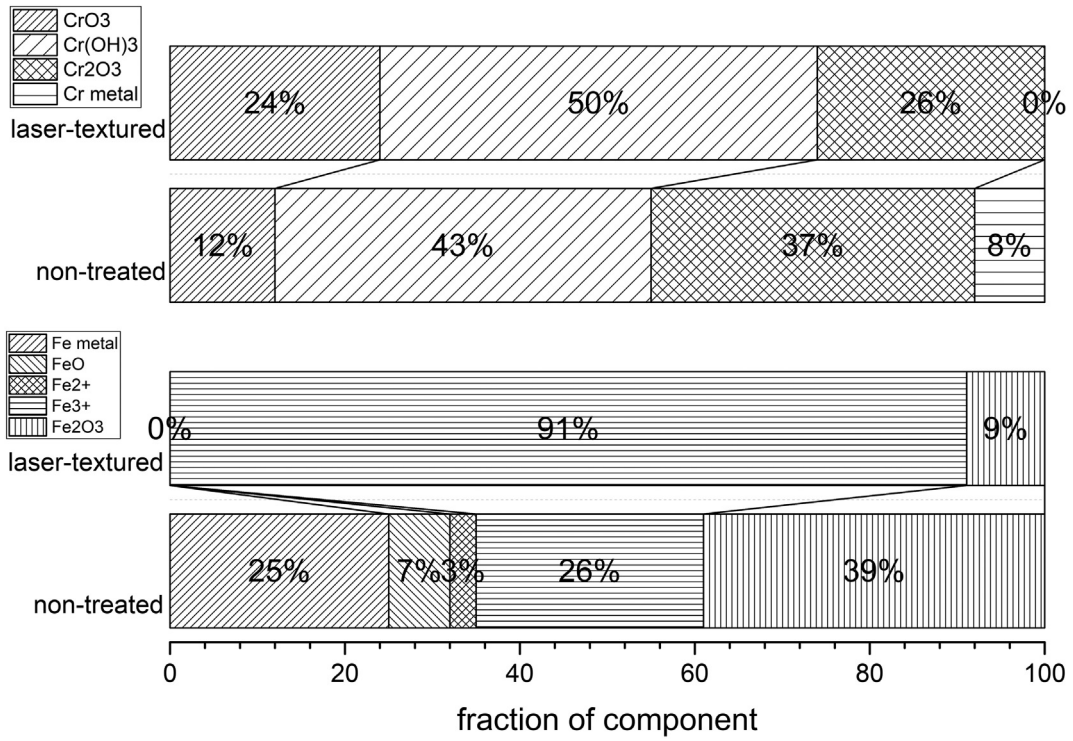

Fig. 5. Fractions of Cr- (top) and Fe-oxide (bottom) components for laser-textured and as-received samples.

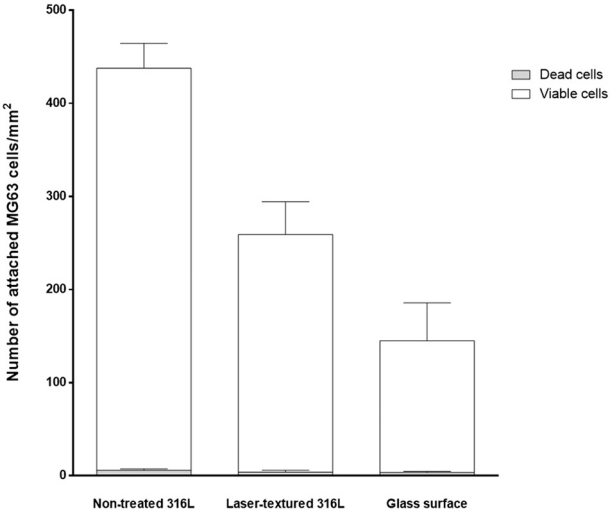

Fig. 6. Adhesion of MG63 cells to the non-treated, laser-textured, and glass samples after 24-hour incubation.

3.4. Cell adhesion, viability, and morphology

We compared the (*i*) cell adhesion pattern, (*ii*) cell viability, and (*iii*) cell morphology, along with exosome formation, of human bone osteosarcoma cells (MG63) on non-treated and laser-textured stainless steel surfaces. As a control, glass disk surfaces were used (see also sections S3 and S4 in Supplementary Material). The presence of adhered cells on the surface, as observed with microscopy, does not automatically suggest that the cells are viable. Therefore, fluorescence microscopy was used to discriminate and count viable and dead, but still adhered cells. A higher number of adhered, viable cells after 24 h incubation were observed on the non-treated sample (Fig. 6). The data in Fig. 6 show the mean number (± standard deviation) of the attached cells per mm^2, where the number of viable and dead cells was investigated in triplicate. The number of attached, viable cells on the non-treated 316L samples is significantly higher in comparison with the number of attached cells on the laser-textured 316L and glass control samples, where the least adhered cells are found ($p < 0.05$). By contrast, the number of dead cells is not significantly different between the non-treated and laser-textured 316L samples ($p > 0.05$).

Viability staining reveals an insignificant number of dead cells (1.4% ± 0.1%) after 24 h on both non-treated and laser-textured stainless-steel surfaces (Figs. 6 and 7a and b), reflecting their non-toxicity. Slightly more (2.5%) dead cells are observed on glass control surface (see Figs. S11 and S12). Note that the absolute number of dead cells (the grey columns in Fig. 5) is similar on the laser-textured and glass surfaces, but the share of the dead cells on the glass surface is higher, since number of the attached cells on the glass surface is lower than on the other two surfaces (the white column in Fig. 6).

Differences in cell distribution and morphology between glass, non-treated and laser-textured surfaces were examined using SEM. From the tested stainless steel samples, we selected the most representative images of cell adhesion and morphology, as shown in Fig. 7 and Fig. 8 (see also additional Figs. S12–S14 for cells on the non-treated surfaces, Figs. S15–S17 for cells on the glass surfaces and Figs. S18–19 for cells on the laser-textured surfaces). The most pronounced differences could be summarised in terms of:

- *Surface distribution* is visible from Figs. 7 and 8. The MG63 cells on the non-treated sample exhibit random orientation on the surface, whereas on the textured surfaces, the attachment pattern is conditioned by the laser-textured morphology in which cells aligned and attached along/on the groves, inside the grooves, and in-between neighbouring grooves. The distribution and the adhesion pattern on control glass are similar to the non-treated surface (see Fig. S15).
- *The shape of the cells* also differs significantly between the laser-textured and non-treated stainless-steel surfaces. The majority of cells on the non-treated surface are polygonal, highly elongated, and flattened with numerous filopodia attached firmly to the substratum surface. This suggests high cellular interaction with the substrate and normal cell growth. Some cells are extremely elongated and spindle-shaped. Furthermore, the number of rounded, non-flattened cells with short filamentous protrusions and anchoring points, indicating poor adhesion and low cellular interactions with the substrate, is small (15% ± 3%). The majority of the polygonal cells are between 30 and 80 ± 5 µm, while the round shaped cells are smaller in size with dimensions between 10 and 20 ± 3 µm (Fig. 8a–c). Similar results are also observed in control samples with the difference that more cells firmly attached to glass, meaning that the cells are more flatten, occupying bigger surface area (see Fig. S16a and b). On the textured surfaces, the attachment pattern is conditioned by the laser-textured morphology, with cells aligned and attached along/on the groves, inside the grooves, and in-between neighbouring grooves (Fig. 8d–f). However, they all have a smaller footprint, are more round-shaped than elongated, and the filamentous protrusions (filopodia) and anchoring points are shorter as for the cells on the non-treated and glass samples. This indicates poorer adhesion and low surface interactions when compared with the non-treated stainless steel samples (Fig. 8a–c).
- *Cell surface morphology and presence of exosomes* is examined on the SEM images. It is clearly visible that the outer cell membranes are covered with microvilli, extracellular vesicles (EVs; i.e., exosomes), and cell tubular interconnections known as tunnelling nanotubes (TNT). Cell surfaces with *hair-like* protrusions (microvilli) and very low amounts of extracellular vesicles are predominantly observed on the non-treated stainless steel and glass samples (Figs. 8c, S17c and d). This is in contrast to the laser-textured surface (Fig. 8d–f), where the amounts of exosomes and microvilli are high. Cluster of exosomes, averaging 250 nm in size are observed.

4. Discussion

4.1. Surface characteristics after laser treatment

When metals are processed by high-fluence laser pulses in air, surface oxidation inevitably accompanies modifications of surface micro- and nanotopography. Altogether, this significantly changes the surface wettability towards (super)hydrophilicity [17,18,31,42]. During and after laser ablation, secondary nanostructures develop on primary microstructures as a consequence of ultra-fast heating, ablation, evaporation and re-deposition from the vaporized phase, and solidification, as has already been reported for 316L stainless steel and titanium by many researchers, including Gregorčič et al. [17,22], Oberringer et al. [34], and Vorobyev and Guo [62]. Cell adhesion, proliferation, migration and filopodial growth have all been correlated with material nanotopography [1,63–65].

Laser texturing influences surface chemistry [17,21,30,31] due to the preferential ablation of some alloy components and oxidation reactions on the surface layer [11,66]. Non-treated 316L samples are covered with a passive, chromium-rich, oxide film that naturally forms on the steel surface. However, laser-texturing in an oxygen-rich environment results in the formation of a thick, high-temperature oxide layer [34,67,68] that may vary in chemical composition, thickness, continuity, and adhesion to the substrate, depending on the pulse fluence [66].

The main observed difference in the chemical composition of the surface layer between the non-treated and laser-textured samples is in the fractions of chromium and iron oxides that formed on the surface. The native oxide on stainless steel consisted mainly of Cr_2O_3 and $Cr(OH)_3$ hydroxide, with smaller amounts of CrO_3 oxide. By contrast, the

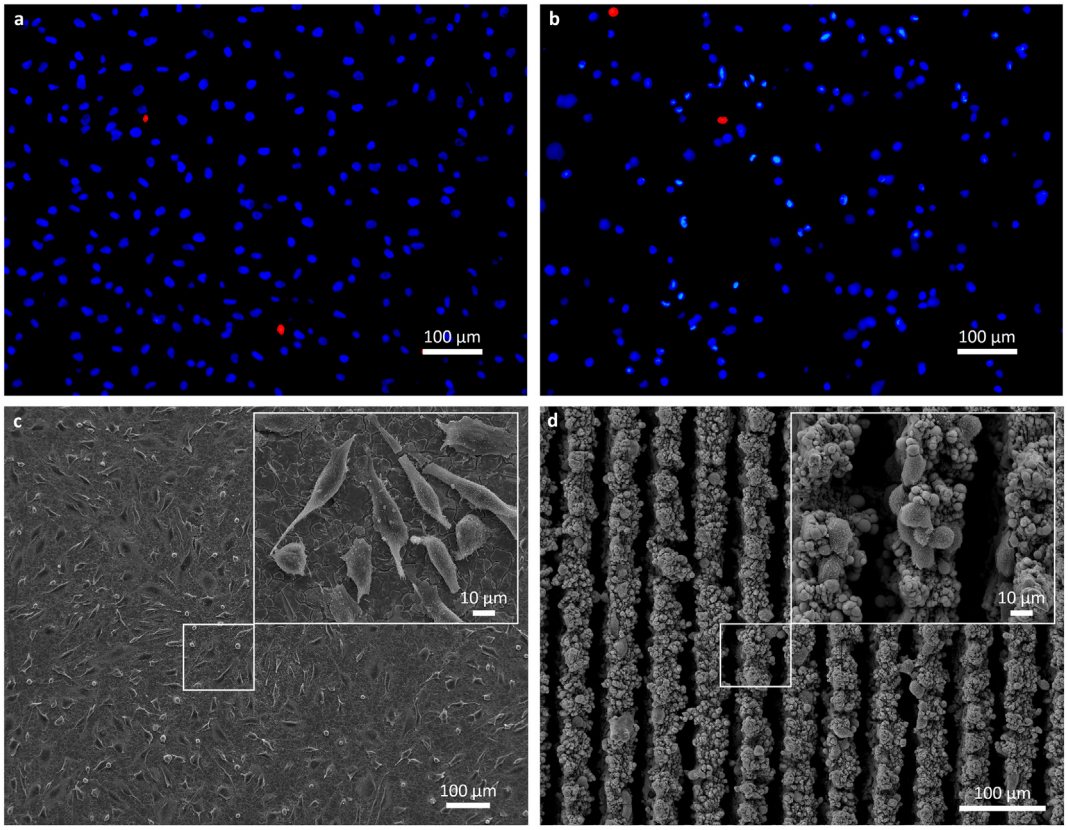

Fig. 7. Representative example of a fluorescence microscopy image used for quantification and of the viability assay results (nuclei of viable cells are blue, while nuclei of dead cells are red) of a (a) non-treated sample and (b) laser-textured sample incubated for 24 h. SEM images of MG63 cell distribution and shapes on a (c) non-treated sample and (d) laser-textured sample. (For interpretation of the references to colour in this figure legend, the reader is referred to the web version of this article.)

high temperatures during laser ablation favoured the formation of hexavalent Cr oxide (CrO_3). The graphic in Fig. 5 highlights the differences in the Cr 2p3/2 high-resolution XPS spectra between the non-treated and laser-textured samples. The main Fe oxide that formed on the surface of the laser-textured samples is Fe_3O_4, while in the case of the native oxide, a mixture of FeO, Fe_3O_4, and Fe_2O_3 oxides is observed.

The non-treated and laser-textured surfaces are both covered with carbon contamination from the environment. This can act as a bioactive component, which can promote early-stage osseointegration and potentially improve biocompatibility. Carbon contamination can decrease the prevalence of corrosion and may reduce CoCr metal particle detachment from the implant surface [32]. However, it should be taken

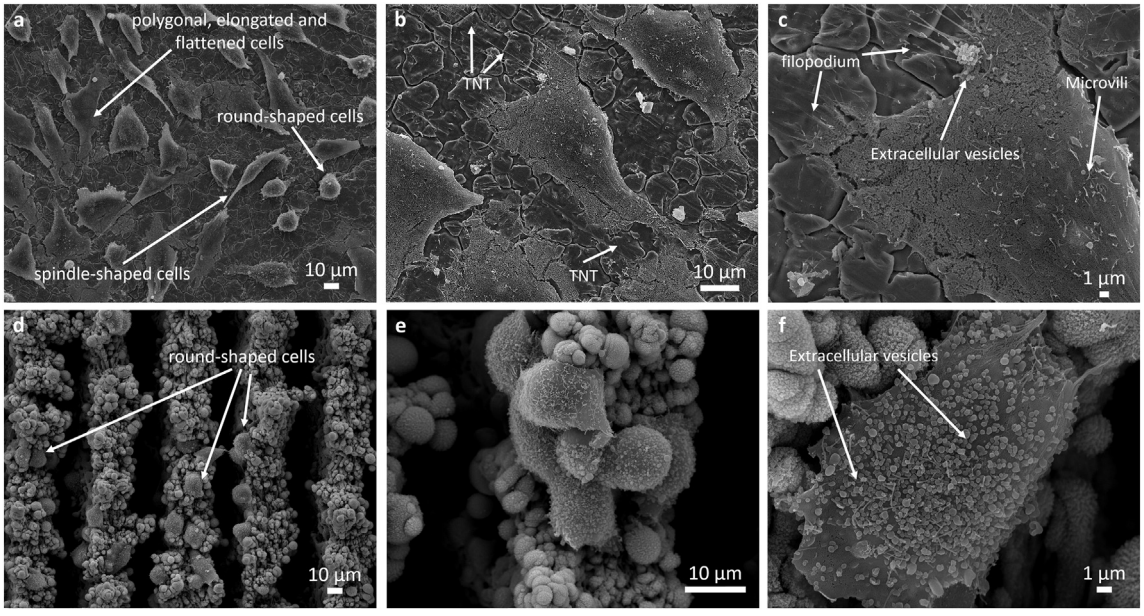

Fig. 8. SEM images of MG63 cell distribution and shapes on a (a–c) non-treated sample and (d–f) laser-textured sample.

into account that the surfaces of the 316 L samples are firstly covered by the adsorbed molecules from the cell culture medium. Therefore, cells initially respond to adsorbed proteins and lipids [15,64]. The adsorption and orientation of these molecules are conditioned by the pH, ionic composition, temperature, functional groups of proteins, and substrate properties [15]. Ultimately, only the uppermost atomic layers of a material which come into contact with the biological environment drive the biofunctionality of the material.

Laser texturing turned our surfaces with an apparent contact angle of around 90° into superhydrophilic, i.e., saturated Wenzel regime. Similar superhydrophilic behaviour immediately following laser processing was reported by other authors using different metals [17,18,32,42,47,69]. They reported the wettability transition towards hydrophobicity or even superhydrophobicity after 1–2 month of surface exposure to atmospheric air. This most probably happens due to surface contamination by organic compounds [31,70–72]. However, in our case all the experiments were performed on surfaces immediately after laser texturing, when the surfaces were still in the superhydrophilic saturated Wenzel regime ($\theta = 0°$).

4.2. Cell adhesion on treated and non-treated surfaces

4.2.1. Cell attachment

Osteoblast-material interactions depend on the surface properties of the material, which determine the extent of adsorption and orientation of the adsorbed molecules, and subsequently the cell behaviour upon contact [15].

We observed more cells on the non-processed, as well as on the laser-textured surfaces compared to the glass samples. There are two possible reasons for this. The first one is high smoothness of the glass, while the second one is low apparent contact angle of glass surfaces (only 20°). It has already been shown that osteoblast-like cells adhere and proliferate better to rough surfaces [73–75]. Different surfaces also adsorb different proteins to different degrees, possibly including those required for cell attachment [76]. Nevertheless, we observed that fewer cells adhere to the rougher laser-textured surface than to the non-treated after 24 h incubation. This may be attributed to the modified surface properties and probably due to the formation of toxic metal oxides. As shown by XPS analysis (Figs. 4 and 5), laser texturing modifies the share of Cr and Fe oxides, turning all the Fe and Cr metals into oxidized forms.

In comparison to the non-processed surface, the laser-textured surface was superhydrophilic and much rougher, with micro/nanotopographic features. This might reduce the attachment efficiency of the cells. Surface wettability is an important factor governing cellular adhesion on surfaces. Cells typically prefer to adhere selectively on hydrophilic regions in the absence and presence of pre-adsorbed proteins [4,77]. Several studies have indicated superior cell attachment and cell spreading on hydrophilic surfaces with contact angles being in the range of 50°–70°, while a decrease in adhesion has been observed for more hydrophilic or hydrophobic surfaces [4,7,15,78]. However, cell behaviour also depends on the cell type and material. For example, Raimbault et al. [79] observed good cell adhesion on titanium despite using surfaces that were no longer hydrophilic. Therefore, the widespread idea that hydrophilic surfaces are better than hydrophobic for biological applications should be treated with caution due to the fact that there is no direct correlation between these two parameters. Additionally, it is difficult to discuss the effect of wettability without considering surface chemistry, topography, and adsorbed molecules from the cell culture medium.

The cell morphology observed on the laser-textured surfaces (i.e., round shapes, smaller footprints, shorter and less tubular protrusions, and abundant exosomes) indicates that stainless-steel surfaces which are textured in an oxygen-containing atmosphere by high-fluence pulses are unfavourable for MG63 cells. Less favourable conditions can be attributed to the altered hydrophilicity of the surface and a micro- and nanotopography that can reduce the points of focal adhesion compared with smoother surfaces. An additional effect may be the presence of different chromium oxides on the surface that do not favour adhesion.

During laser processing, high temperatures favour the formation of hexavalent Cr oxide (CrO_3) which is the most toxic oxidation state of Cr and can be internalised by cells via nonspecific anion transporters, where cellular reductants reduce Cr(VI) into reactive intermediates such as Cr(V), Cr(IV), Cr(III), and reactive oxygen species (ROS), indicating oxidative stress [80–82]. The release of Cr ions can be triggered by chemical dissolution, which is enhanced in protein containing media [83].

The surfaces of laser-textured samples contain a much thicker layer of chromium and iron oxides, particularly toxic Cr(VI), which may also contribute to lower adhesion, morphological changes, oxidative stress, and cell apoptosis. Additionally a higher Cr(VI) ion release may be due to the fact that this high-temperature oxide, although thicker, is also porous.

The native oxide layer found on non-treated samples is, on the other hand, more chemically passive, enables good corrosion resistance (especially Cr_2O_3), is less reactive to biological media, and promotes biocompatibility with the metallic surface [83]. Nonetheless, 24 h exposure may be too short period to give us relevant data about the toxicity of Cr oxides. Thus, additional studies about the role of Cr oxides on cell adhesion for longer exposure times (up to 200 h) should be performed in the future to clarify this effect.

Metal ions released from actively corroding metals are predominantly from oxidized bulk materials whereas passive stainless steel has a much lower ion release, mostly related to chemical or electrochemical dissolution of the surface oxide layer. Stainless steel surface oxide can be dissolved by the reduction of Fe oxides or oxidation processes of the Cr oxide. It is also important to take into consideration correlations between metal release and the adsorption of specific proteins when designing improvements with regards to biocompatibility [84].

Surface topography and roughness also influence cell distribution. The smoother surfaces of non-treated 316L and glass samples are covered with randomly attached cells without any preferential orientation (Figs. 7, 8, and S15), while on the laser-textured samples, the attachment pattern is conditioned by the laser-textured morphology. Most of the cells are aligned and attached along/on the groves, which is in agreement with observations by others [32,33,85–87]. Cell spreading on various materials is better on smooth surfaces compared with rough ones [15]. This well spread, flattened morphology represents good adhesion and is a prerequisite for proliferation [32].

Viability testing revealed only a few dead cells on both surfaces (Fig. 7a and b) and is in agreement with other studies in which laser texturing did not induce cytotoxicity [24,88,89]. However, additional studies with longer exposure durations are needed to understand the adverse effects of laser texturing on cell behaviour and to finally draw such conclusions.

4.2.2. Cell morphology

Cell-material-surface interactions play a crucial role in biomaterial applications, including osseointegration. Cells “show” preferences for certain materials identified by their gross morphological characteristics [90]. MG63 cells incubated on laser-textured surfaces have a different cell surface morphology in comparison with cells on the non-treated and glass samples. Flattened and well-spread cells with extended filopodia are a morphological characteristic of healthy, well adhered cells with high substrate interaction. However, a round shape indicates a sub-optimal (stress) cell state [91,92] usually accompanied by exosome release that are observed as exosome clusters attached to the surface [53]. Cells growing on laser-textured samples have less flattened morphology, which does not allow one to infer any preferential direction for migration. In addition, the cells mainly formed unbranched

filopodia for probing the surface and have poor interaction with the laser-textured surface. Similar results for fibroblast cells were observed by Kenar et al. [32] and Fadeeva et al. [36] who concluded that altered cell behaviour is related to surface topography, since there were no detected alterations in the chemistry of structured surfaces compared with untreated surfaces. Furthermore, the cells on the laser-textured samples have a strong overexpression of exosomes (averaging 250 nm in size), which has not been previously described in the literature on cell-surface interactions.

The observed morphological responses serve as indicator of the efficiency of cell–nanotopography interactions, for which filopodia are critical organelles that may play an instrumental role in the contact-guidance response [87]. On the other hand, Györgyey et al. [88] have not observed any significant differences in adhesion and morphological changes between MG63 cells incubated on laser-ablated titanium surfaces and control sample surfaces. Micro- and nanotopography can affect overall cell behaviour, such as cell adhesion, cell morphology, cell proliferation, cell orientation, and contact guidance. Surface roughness in the range of 10 nm to 10 μm may influence cell behaviour, since this is within the same size range as cells and large biomolecules [93,94]. However, in our case the surface roughness of the laser-textured samples is much higher (> 20 μm) and may not result in such an effect. With respect to the morphological results, it can be assumed that the MG63 cells are more rounded and less elongated on the laser-textured samples, which can be attributed to the different hydrophilicity and (presumably) affinity for adsorption and orientation of biological molecules in comparison with the non-treated samples.

5. Conclusions

We performed laser texturing with high-fluence, nanosecond-laser pulses to produce microchannels covered with hierarchically structured metal oxides on stainless steel. On these surfaces, we studied the initial effects of laser-induced topography, morphology, chemistry, and wettability on MG63-cell attachment and growth. Chemical analysis revealed that the surfaces were covered with thick, high-temperature Fe and Cr oxides containing more potentially toxic Cr hexavalent oxide compared with the native oxide layer on the non-treated samples. Stainless steel micro- and nanotopography resulted in reduced cell adhesion and an altered adhesion pattern and cell morphology indicative of cellular stress, as indicated by the overexpression of exosomes. Also SEM analysis revealed a change in the shape and amount of cellular protrusions and reduced cell spreading, causing the osteoblasts to adopt a rounded shape morphology with a smaller footprint. The submicrometer scale roughness of the non–treated surface favoured the formation of long and numerous filopods and long, flattened, elongated cells with good focal adhesion. The nanostructured oxide surface may be a possible reason for the reduced adhesion and cell stress-indicating gross morphology. Laser-textured surfaces did not affect the overall cell viability after 24 h, but long-term examination is still needed to fully understand the influence of laser-induced (toxic) oxides on cell behaviour. However, the presented results show that osteoblast cells respond to a combination of modified surface topography, roughness, wettability, and chemistry already within 24 h. In this context, further studies should go in the direction of laser texturing under different gas atmospheres (N_2, Ar, and CO_2), since they significantly influence surface chemistry at similar surface topography.

CRediT authorship contribution statement

Matej Hočevar: Conceptualization, Methodology, Investigation, Writing - original draft, Visualization, Formal analysis, Project administration, Funding acquisition. **Barbara Šetina Batič:** Investigation, Visualization, Formal analysis, Writing - review & editing. **Matjaž Godec:** Conceptualization, Funding acquisition. **Veno Kononenko:** Investigation, Formal analysis. **Damjana Drobne:** Investigation, Formal analysis, Writing - review & editing, Funding acquisition. **Peter Gregorčič:** Conceptualization, Methodology, Investigation, Writing - review & editing, Project administration, Supervision, Funding acquisition.

Declaration of competing interest

The authors declare that they have no known competing financial interests or personal relationships that could have appeared to influence the work reported in this paper.

Acknowledgement

The authors acknowledge the financial support from the Slovenian Research Agency (research core funding No. P2-0392, P1-0207, P2-0132 and projects No. Z2-9215, J2-1741, J1-9162, and J2-1729) as well as the support from the Ministry of Education, Science and Sport of the Republic Slovenia and the European Union from the European Regional Development Fund (MARTIN project, No. OP20.03531).

Appendix A. Supplementary data

Supplementary data to this article can be found online at https://doi.org/10.1016/j.surfcoat.2020.125878.

References

[1] M.J.P. Biggs, R.G. Richards, M.J. Dalby, Nanotopographical modification: a regulator of cellular function through focal adhesions, Nanomed. Nanotechnol. Biol. Med. 6 (2010) 619–633, https://doi.org/10.1016/j.nano.2010.01.009.
[2] P.-Y. Wang, S. Ding, H. Sumer, R.C.-B. Wong, P. Kingshott, Heterogeneity of mesenchymal and pluripotent stem cell populations grown on nanogrooves and nanopillars, J. Mater. Chem. B 5 (2017) 7927–7938, https://doi.org/10.1039/C7TB01878A.
[3] R. Vilar, A. Almeida, 2 – laser surface treatment of biomedical alloys, Laser Surf. Modif. Biomater, 2016, pp. 35–75, , https://doi.org/10.1016/B978-0-08-100883-6.00002-2.
[4] Y. Su, C. Luo, Z. Zhang, H. Hermawan, D. Zhu, J. Huang, Y. Liang, G. Li, L. Ren, Bioinspired surface functionalization of metallic biomaterials, J. Mech. Behav. Biomed. Mater. 77 (2018) 90–105, https://doi.org/10.1016/j.jmbbm.2017.08.035.
[5] A. Kurella, N.B. Dahotre, Review paper: surface modification for bioimplants: the role of laser surface engineering, J. Biomater. Appl. 20 (2005) 5–50, https://doi.org/10.1177/0885328205052974.
[6] R.M. Pilliar, Metallic biomaterials, in: R. Narayan (Ed.), Biomed. Mater, Springer US, Boston, MA, 2009, pp. 41–81, , https://doi.org/10.1007/978-0-387-84872-3_2.
[7] D. Waugh, C. Toccaceli, A. Gillett, S. Hodgson, J. Lawrence, Surface treatments to modulate bioadhesion: a critical review, Rev. Adhes. Adhes. 4 (2016) 69–103.
[8] Sepehr Razi, Mahmoud Mollabashi, Khosro Madanipour, Nanosecond laser surface patterning of bio grade 316L stainless steel for controlling its wettability characteristics, Int. J. Opt. Photonics 9 (2015), http://ijop.ir/article-1-184-en.html (AWT_TAG).
[9] B. Ratner, A. Hoffman, Physicochemical surface modification of materials used in medicine, Biomater. Sci. An Introd. to Mater. Med. (2013) 201–218, https://doi.org/10.1016/B978-0-08-087780-8.00027-9.
[10] M.V. Cakir, U. Allenstein, M. Zink, S.G. Mayr, Early adhesion of cells to ferromagnetic shape memory alloys functionalized with plasma assembled biomolecules – a single cell force spectroscopy study, Mater. Des. 158 (2018) 19–27, https://doi.org/10.1016/j.matdes.2018.08.012.
[11] A.Y. Vorobyev, C. Guo, Direct femtosecond laser surface nano/microstructuring and its applications, Laser Photonics Rev. 7 (2013) 385–407, https://doi.org/10.1002/lpor.201200017.
[12] E. Stratakis, A. Ranella, C. Fotakis, Biomimetic micro/nanostructured functional surfaces for microfluidic and tissue engineering applications, Biomicrofluidics 5 (2011) 13411, , https://doi.org/10.1063/1.3553235.
[13] L.R. Jaidev, K. Chatterjee, Surface functionalization of 3D printed polymer scaffolds to augment stem cell response, Mater. Des. 161 (2019) 44–54, https://doi.org/10.1016/j.matdes.2018.11.018.
[14] D. Günther, D. Scharnweber, R. Hess, C. Wolf-Brandstetter, M.G. Holthaus, A.F. Lasagni, 1 - high precision patterning of biomaterials using the direct laser interference patterning technology, in: R. Vilar (Ed.), Laser Surf. Modif. Biomater, Woodhead Publishing, 2016, pp. 3–33, , https://doi.org/10.1016/B978-0-08-100883-6.00001-0.
[15] K. Anselme, Osteoblast adhesion on biomaterials, Biomaterials 21 (2000) 667–681, https://doi.org/10.1016/S0142-9612(99)00242-2.
[16] D.G.W.J. Lawrence, Laser Surface Engineering, Elsevier, Oxford, UK, 2015.
[17] P. Gregorčič, B. Šetina-Batič, M. Hočevar, Controlling the stainless steel surface wettability by nanosecond direct laser texturing at high fluences, Appl. Phys. A

Mater. Sci. Process. (2017) 123, https://doi.org/10.1007/s00339-017-1392-5.
[18] D.V. Ta, A. Dunn, T.J. Wasley, R.W. Kay, J. Stringer, P.J. Smith, C. Connaughton, J.D. Shephard, Nanosecond laser textured superhydrophobic metallic surfaces and their chemical sensing applications, Appl. Surf. Sci. 357 (2015) 248–254, https://doi.org/10.1016/j.apsusc.2015.09.027.
[19] U. Hermens, S.V. Kirner, C. Emonts, P. Comanns, E. Skoulas, A. Mimidis, H. Mescheder, K. Winands, J. Krüger, E. Stratakis, J. Bonse, Mimicking lizard-like surface structures upon ultrashort laser pulse irradiation of inorganic materials, Appl. Surf. Sci. 418 (2017) 499–507, https://doi.org/10.1016/j.apsusc.2016.12.112.
[20] F.A. Müller, C. Kunz, S. Gräf, Bio-inspired functional surfaces based on laser-induced periodic surface structures, Materials (Basel) 9 (2016) 476, https://doi.org/10.3390/ma9060476.
[21] Č. Donik, A. Kocijan, I. Paulin, M. Hočevar, P. Gregorčič, M. Godec, Improved biodegradability of Fe–Mn alloy after modification of surface chemistry and topography by a laser ablation, Appl. Surf. Sci. 453 (2018), https://doi.org/10.1016/j.apsusc.2018.05.066.
[22] P. Gregorčič, M. Zupančič, I. Golobič, Scalable surface microstructuring by a fiber laser for controlled nucleate boiling performance of high- and low-surface-tension fluids, Sci. Rep. 8 (2018) 7461, https://doi.org/10.1038/s41598-018-25843-5.
[23] E. Stratakis, A. Ranella, M. Farsari, C. Fotakis, Laser-based micro/nanoengineering for biological applications, Prog. Quantum Electron. 33 (2009) 127–163, https://doi.org/10.1016/j.pquantelec.2009.06.001.
[24] E. Fadeeva, A. Deiwick, B. Chichkov, S. Schlie-Wolter, Impact of laser-structured biomaterial interfaces on guided cell responses, Interf. Focus 4 (2014) 20130048, , https://doi.org/10.1098/rsfs.2013.0048.
[25] S.V. Kirner, U. Hermens, A. Mimidis, E. Skoulas, C. Florian, F. Hischen, C. Plamadeala, W. Baumgartner, K. Winands, H. Mescheder, J. Krüger, J. Solis, J. Siegel, E. Stratakis, J. Bonse, Mimicking bug-like surface structures and their fluid transport produced by ultrashort laser pulse irradiation of steel, Appl. Phys. A Mater. Sci. Process. 123 (2017) 754, https://doi.org/10.1007/s00339-017-1317-3.
[26] V. Zorba, E. Stratakis, M. Barberoglou, E. Spanakis, P. Tzanetakis, S.H. Anastasiadis, C. Fotakis, Biomimetic artificial surfaces quantitatively reproduce the water repellency of a lotus leaf, Adv. Mater. 20 (2008) 4049+, https://doi.org/10.1002/adma.200800651.
[27] W. Barthlott, C. Neinhuis, Purity of the sacred lotus, or escape from contamination in biological surfaces, Planta 202 (1997) 1–8, https://doi.org/10.1007/s004250050096.
[28] E. Skoulas, A. Manousaki, C. Fotakis, E. Stratakis, Biomimetic surface structuring using cylindrical vector femtosecond laser beams, Sci. Rep. 7 (2017) 45114, , https://doi.org/10.1038/srep45114.
[29] S. Sethi, L. Ge, L. Ci, P.M. Ajayan, A. Dhinojwala, Gecko-inspired carbon nanotube-based self-cleaning adhesives, Nano Lett. 8 (2008) 822–825, https://doi.org/10.1021/nl0727765.
[30] S. Kirner, T. Wirth, H. Sturm, J. Krüger, J. Bonse, Nanometer-resolved chemical analyses of femtosecond laser-induced periodic surface structures on titanium, J. Appl. Phys. 122 (2017) 104901.
[31] P. Gregorčič, Comment on "Bioinspired reversible switch between underwater superoleophobicity/superaerophobicity and oleophilicity/aerophilicity and improved antireflective property on the nanosecond laser-ablated superhydrophobic titanium surfaces", ACS Appl. Mater. Interfaces (2020), https://doi.org/10.1021/acsami.9b23462.
[32] H. Kenar, E. Akman, E. Kacar, A. Demir, H. Park, H. Abdul-Khaliq, C. Aktas, E. Karaoz, Femtosecond laser treatment of 316L improves its surface nanoroughness and carbon content and promotes osseointegration: an in vitro evaluation, Colloids Surf. B: Biointerfaces 108 (2013) 305–312, https://doi.org/10.1016/j.colsurfb.2013.02.039.
[33] M. Martínez-Calderon, M. Manso-Silván, A. Rodríguez, M. Gómez-Aranzadi, J.P. García-Ruiz, S.M. Olaizola, R.J. Martín-Palma, Surface micro- and nano-texturing of stainless steel by femtosecond laser for the control of cell migration, Sci. Rep. 6 (2016) 36296, , https://doi.org/10.1038/srep36296.
[34] M. Oberringer, E. Akman, J. Lee, W. Metzger, C.K. Akkan, E. Kacar, A. Demir, H. Abdul-Khaliq, N. Pütz, G. Wennemuth, T. Pohlemann, M. Veith, C. Aktas, Reduced myofibroblast differentiation on femtosecond laser treated 316LS stainless steel, Mater. Sci. Eng. C 33 (2013) 901–908, https://doi.org/10.1016/j.msec.2012.11.018.
[35] S. Schlie, E. Fadeeva, A. Koroleva, A. Ovsianikov, J. Koch, A. Ngezahayo, B.N. Chichkov, Laser-based nanoengineering of surface topographies for biomedical applications, Photonics Nanostruct. Fundam. Appl. 9 (2011) 159–162, https://doi.org/10.1016/j.photonics.2010.09.006.
[36] E. Fadeeva, S. Schlie, J. Koch, B.N. Chichkov, Selective cell control by surface structuring for orthopedic applications, J. Adhes. Sci. Technol. 24 (2010) 2257–2270, https://doi.org/10.1163/016942410X508000.
[37] T. Nuutinen, M. Silvennoinen, K. Päiväsaari, P. Vahimaa, Control of cultured human cells with femtosecond laser ablated patterns on steel and plastic surfaces, Biomed. Microdevices 15 (2013) 279–288, https://doi.org/10.1007/s10544-012-9726-8.
[38] C.-W. Chan, L. Carson, G.C. Smith, A. Morelli, S. Lee, Enhancing the antibacterial performance of orthopaedic implant materials by fibre laser surface engineering, Appl. Surf. Sci. 404 (2017) 67–81, https://doi.org/10.1016/j.apsusc.2017.01.233.
[39] A.H.A. Lutey, L. Gemini, L. Romoli, G. Lazzini, F. Fuso, M. Faucon, R. Kling, Towards laser-textured antibacterial surfaces, Sci. Rep. 8 (2018) 10112, , https://doi.org/10.1038/s41598-018-28454-2.
[40] N. Epperlein, F. Menzel, K. Schwibbert, R. Koter, J. Bonse, J. Sameith, J. Krüger, J. Toepel, Influence of femtosecond laser produced nanostructures on biofilm growth on steel, Appl. Surf. Sci. 418 (2017) 420–424, https://doi.org/10.1016/j.apsusc.2017.02.174.
[41] V. Selvamani, A. Zareei, A. Elkashif, M.K. Maruthamuthu, S. Chittiboyina, D. Delisi, Z. Li, L. Cai, V.G. Pol, M.N. Seleem, R. Rahimi, Hierarchical micro/mesoporous copper structure with enhanced antimicrobial property via laser surface texturing, Adv. Mater. Interfaces 7 (2020) 1901890, , https://doi.org/10.1002/admi.201901890.
[42] U. Trdan, M. Hočevar, P. Gregorčič, Transition from superhydrophilic to superhydrophobic state of laser textured stainless steel surface and its effect on corrosion resistance, Corros. Sci. 123 (2017), https://doi.org/10.1016/j.corsci.2017.04.005.
[43] S. Razi, K. Madanipour, M. Mollabashi, Improving the hydrophilicity of metallic surfaces by nanosecond pulsed laser surface modification, J. Laser Appl. 27 (2015) 42006.
[44] Y. Cai, W. Chang, X. Luo, A.M.L. Sousa, K.H.A. Lau, Y. Qin, Superhydrophobic structures on 316L stainless steel surfaces machined by nanosecond pulsed laser, Precis. Eng. (2018), https://doi.org/10.1016/j.precisioneng.2018.01.004.
[45] S. Razi, M. Mollabashi, K. Madanipour, Laser processing of metallic biomaterials: an approach for surface patterning and wettability control, Eur. Phys. J. Plus. 130 (2015) 247, https://doi.org/10.1140/epjp/i2015-15247-5.
[46] P. Gregorčič, M. Conradi, L. Hribar, M. Hočevar, Long-term influence of laser-processing parameters on (super)hydrophobicity development and stability of stainless-steel surfaces, Materials (Basel) 11 (2018), https://doi.org/10.3390/ma11112240.
[47] A.-M. Kietzig, S.G. Hatzikiriakos, P. Englezos, Patterned superhydrophobic metallic surfaces, Langmuir 25 (2009) 4821–4827, https://doi.org/10.1021/la8037582.
[48] M. Može, M. Zupančič, M. Hočevar, I. Golobič, P. Gregorčič, Surface chemistry and morphology transition induced by critical heat flux incipience on laser-textured copper surfaces, Appl. Surf. Sci. 490 (2019) 220–230, https://doi.org/10.1016/j.apsusc.2019.06.068.
[49] M.P. Fiorucci, A.J. López, A. Ramil, Surface modification of Ti6Al4V by nanosecond laser ablation for biomedical applications, J. Phys. Conf. Ser. 605 (2015) 12022http://stacks.iop.org/1742-6596/605/i=1/a=012022.
[50] J. Gabzdyl, Fibre lasers make their mark, Nat. Photonics 2 (2008) 21–23, https://doi.org/10.1038/nphoton.2007.268.
[51] A. Mogilner, B. Rubinstein, The physics of filopodial protrusion, Biophys. J. 89 (2005) 782–795, https://doi.org/10.1529/biophysj.104.056515.
[52] Y. Zhang, Y. Liu, H. Liu, W.H. Tang, Exosomes: biogenesis, biologic function and clinical potential, Cell Biosci. 9 (2019) 19, https://doi.org/10.1186/s13578-019-0282-2.
[53] M. Saeed-Zidane, L. Linden, D. Salilew-Wondim, E. Held, C. Neuhoff, E. Tholen, M. Hoelker, K. Schellander, D. Tesfaye, Cellular and exosome mediated molecular defense mechanism in bovine granulosa cells exposed to oxidative stress, PLoS One 12 (2017) e0187569, , https://doi.org/10.1371/journal.pone.0187569.
[54] C.A. Schneider, W.S. Rasband, K.W. Eliceiri, NIH image to ImageJ: 25 years of image analysis, Nat. Methods 9 (2012) 671–675 http://www.ncbi.nlm.nih.gov/pmc/articles/PMC5554542/.
[55] B.P. Payne, M.C. Biesinger, N.S. McIntyre, X-ray photoelectron spectroscopy studies of reactions on chromium metal and chromium oxide surfaces, J. Electron Spectros. Relat. Phenomena 184 (2011) 29–37, https://doi.org/10.1016/j.elspec.2010.12.001.
[56] T. Yamashita, P. Hayes, Analysis of XPS spectra of Fe2+ and Fe3+ ions in oxide materials, Appl. Surf. Sci. 254 (2008) 2441–2449, https://doi.org/10.1016/j.apsusc.2007.09.063.
[57] M.C. Biesinger, C. Brown, J.R. Mycroft, R.D. Davidson, N.S. McIntyre, X-ray photoelectron spectroscopy studies of chromium compounds, Surf. Interface Anal. 36 (2004) 1550–1563, https://doi.org/10.1002/sia.1983.
[58] G. McHale, N.J. Shirtcliffe, M.I. Newton, Super-hydrophobic and super-wetting surfaces: analytical potential? Analyst 129 (2004) 284–287, https://doi.org/10.1039/b400567h.
[59] A. Marmur, Soft contact: measurement and interpretation of contact angles, Soft Matter 2 (2006) 12–17, https://doi.org/10.1039/B514811C.
[60] A. Marmur, Hydro- hygro- oleo- omni-phobic? Terminology of wettability classification, Soft Matter 8 (2012) 6867–6870, https://doi.org/10.1039/C2SM25443C.
[61] J. Drelich, E. Chibowski, D.D. Meng, K. Terpilowski, Hydrophilic and superhydrophilic surfaces and materials, Soft Matter 7 (2011) 9804–9828, https://doi.org/10.1039/C1SM05849E.
[62] A.Y. Vorobyev, C. Guo, Femtosecond laser structuring of titanium implants, Appl. Surf. Sci. 253 (2007) 7272–7280, https://doi.org/10.1016/j.apsusc.2007.03.006.
[63] L. Yang, H. Liu, Y. Lin, Biomaterial nanotopography-mediated cell responses: experiment and modeling, Int. J. Smart Nano Mater. 5 (2014) 227–256, https://doi.org/10.1080/19475411.2014.995744.
[64] K. Anselme, P. Davidson, A.M. Popa, M. Giazzon, M. Liley, L. Ploux, The interaction of cells and bacteria with surfaces structured at the nanometre scale, Acta Biomater. 6 (2010) 3824–3846, https://doi.org/10.1016/j.actbio.2010.04.001.
[65] J.R. Jones, Observing cell response to biomaterials, Mater. Today 9 (2006) 34–43, https://doi.org/10.1016/S1369-7021(06)71741-2.
[66] B. Szubzda, A. Antończak, P. Kozioł, Ł. Łazarek, B. Stępak, K. Łęcka, A. Szmaja, M. Ozimek, Corrosion resistance of the AISI 304, 316 and 321 stainless steel surfaces modified by laser, IOP Conf. Ser. Mater. Sci. Eng. 113 (2016) 12017, , https://doi.org/10.1088/1757-899x/113/1/012017.
[67] H. L, L. J., P.Y. F., C.K. S, L.G. C, Z.H. Y, Enhanced human osteoblast cell adhesion and proliferation on 316 LS stainless steel by means of CO2 laser surface treatment, J. Biomed. Mater. Res. Part B Appl. Biomater. 73B (2004) 148–156, https://doi.org/10.1002/jbm.b.30194.
[68] A. Bandyopadhyay, H. Sahasrabudhe, S. Bose, R Vilar (Ed.), 6 - Laser Surface Modification of Metallic Biomaterials, Woodhead Publishing, 2016, pp. 175–195, , https://doi.org/10.1016/B978-0-08-100883-6.00006-X.
[69] Y.C. Guan, F.F. Luo, G.C. Lim, M.H. Hong, H.Y. Zheng, B. Qi, Fabrication of metallic

surfaces with long-term superhydrophilic property using one-stop laser method, Mater. Des. 78 (2015) 19–24, https://doi.org/10.1016/j.matdes.2015.04.021.
[70] L.B. Boinovich, A.M. Emelyanenko, K.A. Emelyanenko, A.G. Domantovsky, A.A. Shiryaev, Comment on "Nanosecond laser textured superhydrophobic metallic surfaces and their chemical sensing applications" by Duong V. Ta, Andrew Dunn, Thomas J. Wasley, Robert W. Kay, Jonathan Stringer, Patrick J. Smith, Colm Connaughton, Jonathan D. Shephard, Appl. Surf. Sci. 379 (2016) 111–113, https://doi.org/10.1016/j.apsusc.2016.04.056.
[71] J. Long, M. Zhong, P. Fan, D. Gong, H. Zhang, Wettability conversion of ultrafast laser structured copper surface, J. Laser Appl. 27 (2015) S29107, https://doi.org/10.2351/1.4906477.
[72] Z. Yang, X. Liu, Y. Tian, Insights into the wettability transition of nanosecond laser ablated surface under ambient air exposure, J. Colloid Interface Sci. 533 (2019) 268–277, https://doi.org/10.1016/j.jcis.2018.08.082.
[73] J.Y. Martin, Z. Schwartz, T.W. Hummert, D.M. Schraub, J. Simpson, J. Lankford Jr., D.D. Dean, D.L. Cochran, B.D. Boyan, Effect of titanium surface roughness on proliferation, differentiation, and protein synthesis of human osteoblast-like cells (MG63), J. Biomed. Mater. Res. 29 (1995) 389–401, https://doi.org/10.1002/jbm.820290314.
[74] S. Lavenus, P. Pilet, J. Guicheux, P. Weiss, G. Louarn, P. Layrolle, Behaviour of mesenchymal stem cells, fibroblasts and osteoblasts on smooth surfaces, Acta Biomater. 7 (2011) 1525–1534, https://doi.org/10.1016/j.actbio.2010.12.033.
[75] K. Rafiee, H. Naffakh-Moosavy, E. Tamjid, The effect of laser frequency on roughness, microstructure, cell viability and attachment of Ti6Al4V alloy, Mater. Sci. Eng. C 109 (2020) 110637, , https://doi.org/10.1016/j.msec.2020.110637.
[76] K. Rechendorff, M.B. Hovgaard, M. Foss, V.P. Zhdanov, F. Besenbacher, Enhancement of protein adsorption induced by surface roughness, Langmuir 22 (2006) 10885–10888, https://doi.org/10.1021/la0621923.
[77] L. Hao, J. Lawrence, Laser Surface Treatment of Bio-implant Materials, Laser Surf. Treat. Bio-Implant Mater, (2006), pp. 1–211, https://doi.org/10.1002/0470033975.
[78] D.P. Dowling, I.S. Miller, M. Ardhaoui, W.M. Gallagher, Effect of surface wettability and topography on the adhesion of osteosarcoma cells on plasma-modified polystyrene, J. Biomater. Appl. 26 (2011) 327–347, https://doi.org/10.1177/0885328210372148.
[79] O. Raimbault, S. Benayoun, K. Anselme, C. Mauclair, T. Bourgade, A.-M. Kietzig, P.-L. Girard-Lauriault, S. Valette, C. Donnet, The effects of femtosecond laser-textured Ti-6Al-4V on wettability and cell response, Mater. Sci. Eng. C 69 (2016) 311–320, https://doi.org/10.1016/j.msec.2016.06.072.
[80] J. Das, A. Sarkar, P.C. Sil, Hexavalent chromium induces apoptosis in human liver (HepG2) cells via redox imbalance, Toxicol. Rep. 2 (2015) 600–608, https://doi.org/10.1016/j.toxrep.2015.03.013.
[81] C.M. Thompson, Y. Fedorov, D.D. Brown, M. Suh, D.M. Proctor, L. Kuriakose, L.C. Haws, M.A. Harris, Assessment of Cr(VI)-induced cytotoxicity and genotoxicity using high content analysis, PLoS One 7 (2012) e42720, , https://doi.org/10.1371/journal.pone.0042720.
[82] G. De Mattia, M.C. Bravi, O. Laurenti, O. De Luca, A. Palmeri, A. Sabatucci, G. Mendico, A. Ghiselli, Impairment of cell and plasma redox state in subjects professionally exposed to chromium, Am. J. Ind. Med. 46 (2004) 120–125, https://doi.org/10.1002/ajim.20044.
[83] P. Silva-Bermudez, S.E. Rodil, An overview of protein adsorption on metal oxide coatings for biomedical implants, Surf. Coat. Technol. 233 (2013) 147–158, https://doi.org/10.1016/j.surfcoat.2013.04.028.
[84] Y.S. Hedberg, I. Odnevall Wallinder, Metal release from stainless steel in biological environments: a review, Biointerphases 11 (2015) 18901, , https://doi.org/10.1116/1.4934628.
[85] K.T. Voisey, C.A. Scotchford, L. Martin, H.S. Gill, Effect of Q-switched laser surface texturing of titanium on osteoblast cell response, Phys. Procedia 56 (2014) 1126–1135, https://doi.org/10.1016/j.phpro.2014.08.027.
[86] M. Wang, Y. Lu, Nano patterned PDMS for periodontal ligament fibroblast culture, Surf. Coat. Technol. 204 (2009) 525–530, https://doi.org/10.1016/j.surfcoat.2009.08.035.
[87] C.J. Bettinger, R. Langer, J.T. Borenstein, Engineering substrate micro- and nanotopography to control cell function, Angew. Chem. Int. Ed. Eng. 48 (2009) 5406–5415, https://doi.org/10.1002/anie.200805179.
[88] Á. Györgyey, K. Ungvári, G. Kecskeméti, J. Kopniczky, B. Hopp, A. Oszkó, I. Pelsöczi, Z. Rakonczay, K. Nagy, K. Turzó, Attachment and proliferation of human osteoblast-like cells (MG-63) on laser-ablated titanium implant material, Mater. Sci. Eng. C 33 (2013) 4251–4259, https://doi.org/10.1016/j.msec.2013.06.020.
[89] M. Vehse, M. Löbler, K.-P. Schmitz, H. Seitz, Laser Induced Surface Structure on Stainless Steel Influences Cell Viability, (2012), https://doi.org/10.1515/bmt-2012-4007.
[90] C.A. Mullen, M.G. Haugh, M.B. Schaffler, R.J. Majeska, L.M. McNamara, Osteocyte differentiation is regulated by extracellular matrix stiffness and intercellular separation, J. Mech. Behav. Biomed. Mater. 28 (2013) 183–194, https://doi.org/10.1016/j.jmbbm.2013.06.013.
[91] A. Ranella, M. Barberoglou, S. Bakogianni, C. Fotakis, E. Stratakis, Tuning cell adhesion by controlling the roughness and wettability of 3D micro/nano silicon structures, Acta Biomater. 6 (2010) 2711–2720, https://doi.org/10.1016/j.actbio.2010.01.016.
[92] A.K.M.R.H. Chowdhury, A. Tavangar, B. Tan, K. Venkatakrishnan, Biofunctionalized 3-D carbon nano-network platform for enhanced fibroblast cell adhesion, Sci. Rep. 7 (2017) 44250, https://doi.org/10.1038/srep44250.
[93] J.I. Rosales-Leal, M.A. Rodríguez-Valverde, G. Mazzaglia, P.J. Ramón-Torregrosa, L. Díaz-Rodríguez, O. García-Martínez, M. Vallecillo-Capilla, C. Ruiz, M.A. Cabrerizo-Vílchez, Effect of roughness, wettability and morphology of engineered titanium surfaces on osteoblast-like cell adhesion, Colloids Surf. A Physicochem. Eng. Asp. 365 (2010) 222–229, https://doi.org/10.1016/j.colsurfa.2009.12.017.
[94] T. Sjöström, G. Lalev, J.P. Mansell, B. Su, Initial attachment and spreading of MG63 cells on nanopatterned titanium surfaces via through-mask anodization, Appl. Surf. Sci. 257 (2011) 4552–4558, https://doi.org/10.1016/j.apsusc.2010.11.064.

Supplementary Material

The interaction between the osteosarcoma cell and stainless steel surface, modified by high-fluence, nanosecond laser pulses

Matej Hočevar[1], Barbara Šetina Batič[1], Matjaž Godec[1], Veno Kononenko[2], Damjana Drobne[2], Peter Gregorčič[1,3]*

[1]Institute of Metals and Technology, Lepi pot 11, 1000 Ljubljana, Slovenia

[2]Department of Biology, Biotechnical Faculty, University of Ljubljana, Večna pot 111, 1000 Ljubljana, Slovenia

[3]Faculty of Mechanical Engineering, University of Ljubljana, Aškerčeva 6, 1000 Ljubljana, Slovenia

Corresponding author:

**e-mail: peter.gregorcic@fs.uni-lj.si, +386 1 477 1 172*

Table of Contents:

S1 Surface morphology and topography measurements

As explained in the main manuscript, surface morphology, topography, and roughness of the non-treated and laser-textured 316L samples were examined by using SEM (surface morphology imaging) and IFM (3D surface roughness measurements). Surface topography is a three-dimensional parameter and describes the morphological pattern of a surface. Commonly used surface roughness parameters usually describe only one aspect of the surface topography, surface height variation (R_a and R_q, R_z, R_{max}), or spatial distribution and shape of the surface features (R_{sk}, R_{ku}, S_{ds}) [S1]. However, surfaces with clearly different structures can have similar R_a values. Additionally, the topography can significantly vary depending on the scale of the analysis.

Figure S1 reveals that surface of the non-treated sample exhibits a typical grain-structured-like morphology with very smooth grains (< 20 µm) separated with narrow crevices (< 1.5 µm).

On the surface of the laser-textured sample, a hierarchical micro- and nanostructured high-temperature oxide is observed at higher magnifications. As visible in Figure S2, the oxide appears on the surface as hairy nanostructured layer reminiscent of a dandelion light. When removed due to different causes, native oxide is forming instead.

Surface area roughness (S_a) reveals that the laser-textured sample is much rougher due to the laser-induced morphology. However, on the laser-textured surface due to the desired topography the roughness along laser path is different than the roughness perpendicular to the laser scanning path. To enable better comparison between the non-treated and laser-textured surfaces, the arithmetic average roughness (R_a) and mean peak to valley height of the roughness profile (R_z) is also evaluated on both surfaces. However, in some cases R_a is not a good measure of roughness due to specific topography of a surface (topography, oriented in one direction). On the non-treated surface, without any preferential topography, R_a was measured perpendicular (R_{ap}) and parallel (R_{al}) with respect to the sample (Figures S3-S4), while on the laser-textured sample R_a was measured perpendicular (R_{ap}) and parallel (R_{al}) to the direction of the laser-texturing.

No differences in surface roughness are observed on the non-treated sample at different directions of measurement. On the other hand, significant difference is observed on the laser-textured sample (Table S1). Laser-textured sample is much rougher perpendicular to the laser-texturing, while parallel R_{al} is lower. On the laser-textured surfaces, nanoroughness – as additional level of roughness – appears due to formation of specific high-temperature oxides.

A cross-section of both samples is shown in Figure S5 for better visual comparison of the surface profiles on the non-treated and the laser-textured samples.

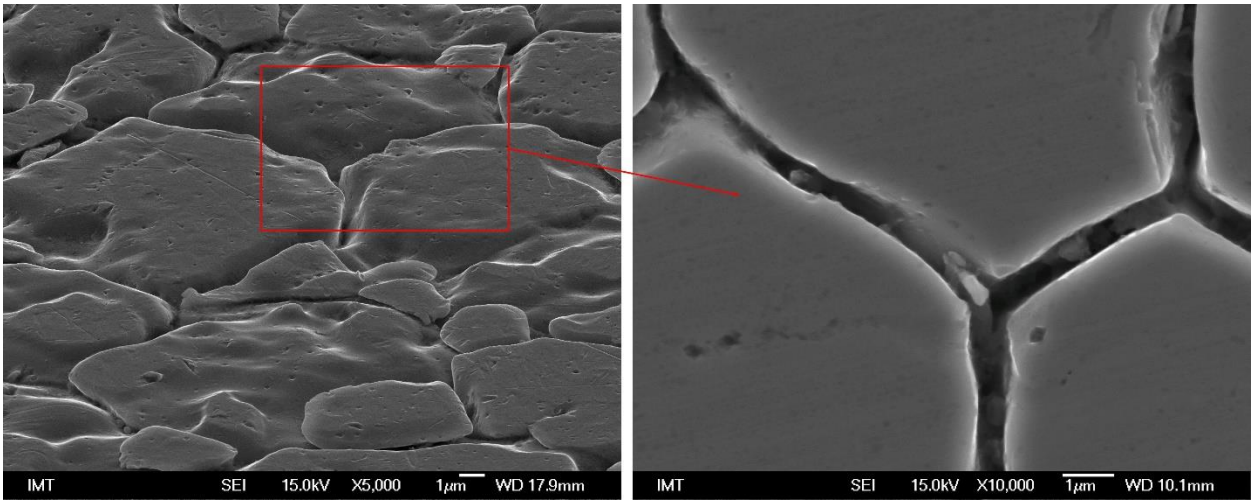

Figure S1. *SEM image of the tilted (65°) non-treated sample.*

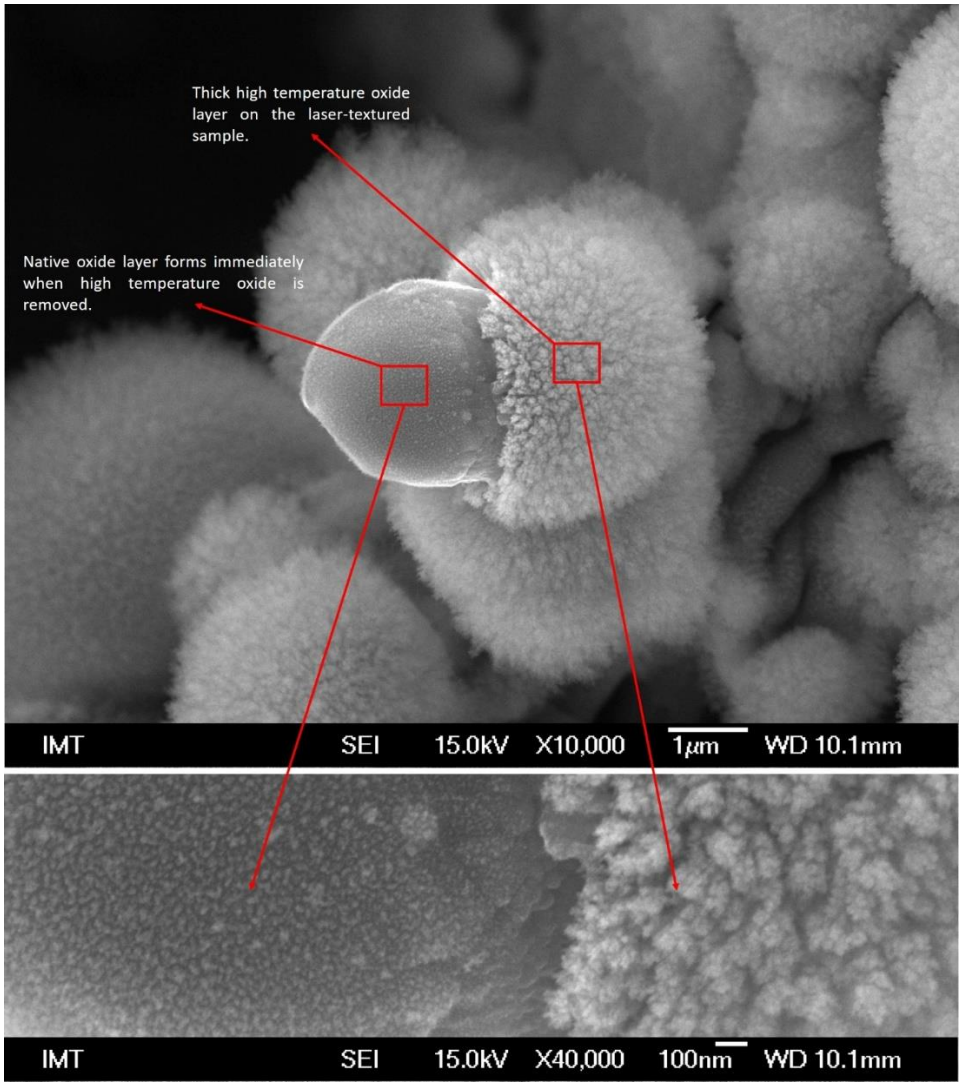

Figure S2. *SEM image of the laser-textured surface and surface oxide layer, induced by laser texturing.*

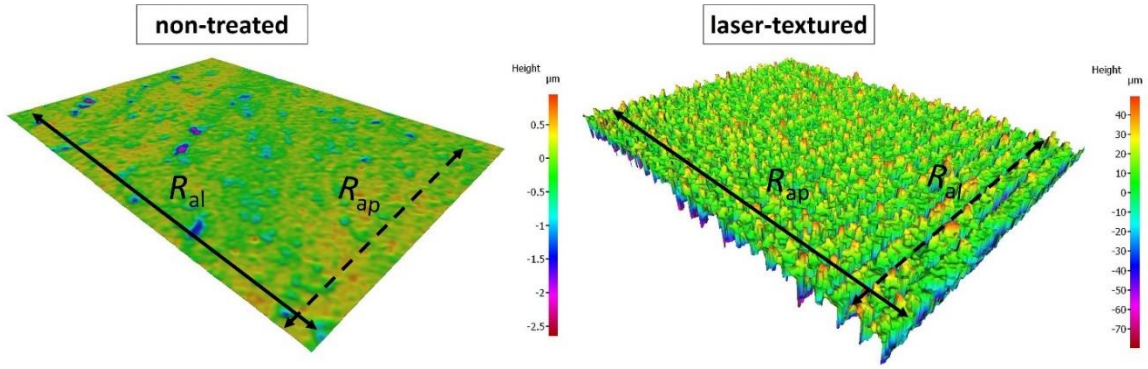

Figure S3. *IFM 3D height image of the non-treated and laser-textured surfaces with roughness measurements.*

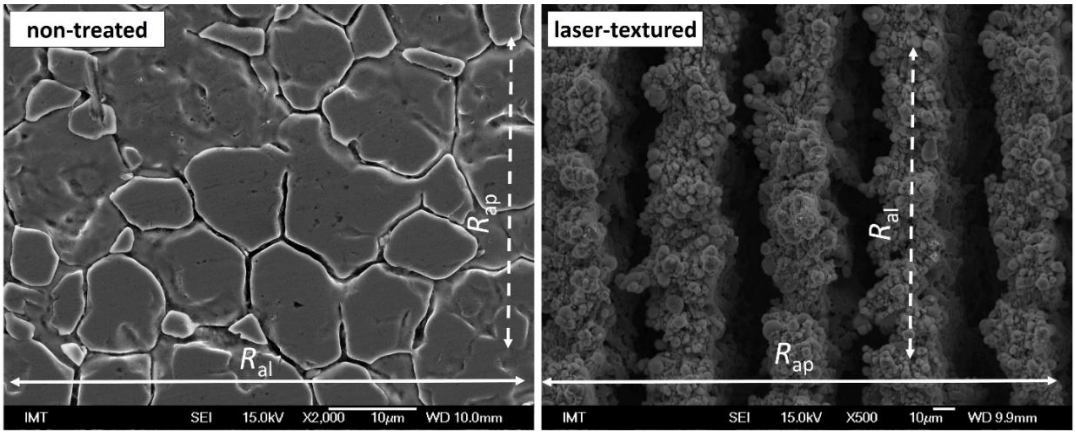

Figure S4. *SEM images of the non-treated and laser-textured surface with roughness measurements.*

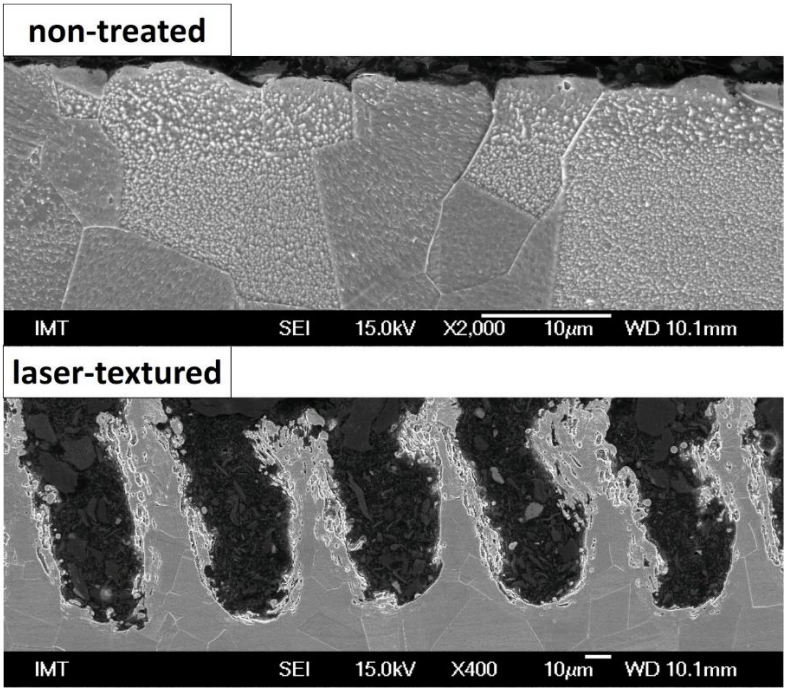

Figure S5. *Cross-section SEM images of the non-treated and laser-textured surface.*

Table S1. *Surface roughness parameter (R_a and R_z) values.*

Sample	R_{ap} (µm)	R_{al} (µm)	R_{zp} (µm)	R_{zl} (µm)
316L, non-treated	0.19 ± 0.02	0.19 ± 0.03	1.71 ± 0.39	1.66 ± 0.39
316L, laser-textured	16.1 ± 0.6	8.15 ± 0.7	113 ± 1.6	43.1 ± 4.8

S2 Surface chemistry

Table S2 provides numerical values of the O element, measured by EDS on the points, shown in Figure 2 in the main text. Lower values on the non-treated sample indicate that the oxide layer is significantly thinner compared to the laser-textured sample.

Table S2. *EDS O element analyses on the non-treated and laser-textured surface (wt %).*

	Sample	
Measurement point	**Non-treated**	**Laser-textured**
1	0	27
2	0	13
3	0	1
4	1	7
5	0	7
6	0	9
7	1	16
8	0	16
9	0	34
10	0	36

S3 Fluorescence microscopy imaging (quantification and viability assay)

To quantify the number of cell adhered and their viability, the samples with attached cells were stained using Hoechst 33342 (stains the nuclei of all cells blue) and Propidium iodide (stains the nuclei of the non-viable cells and cells with damaged plasmalemma) red. Quantitative analysis of the density of attached cells and cell viability was performed using ImageJ software. After 24 h of incubation high number of adhered, viable cells were observed on both the non-treated (Figures

S6-S7) and the laser-textured (Figures S8-S9) samples compared to glass controls, where less adhered cells are observed (FS10-11). This indicates good performance of both stainless-steel surfaces after short-term (24 h) adhesion experiment.

The majority of cells on the non-treated surface are polygonal, highly elongated, and flattened making the nucleus look larger than on the laser-textured samples with smaller, more round-shaped cells. This effect is additionally amplified on the laser-textured surfaces where some cells are out of focus due to high roughness of the sample.

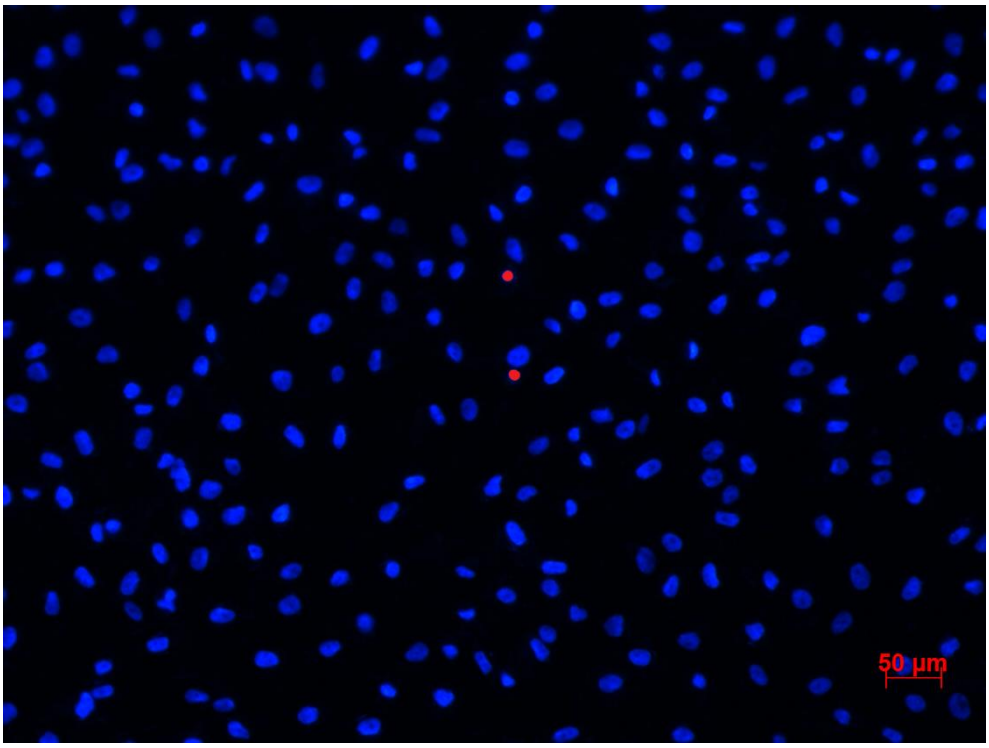

Figure S6. *Fluorescence microscopy image of MG63 cells incubated for 24 h on the non-treated sample (nuclei of viable cells are blue, while nuclei of dead cells are red).*

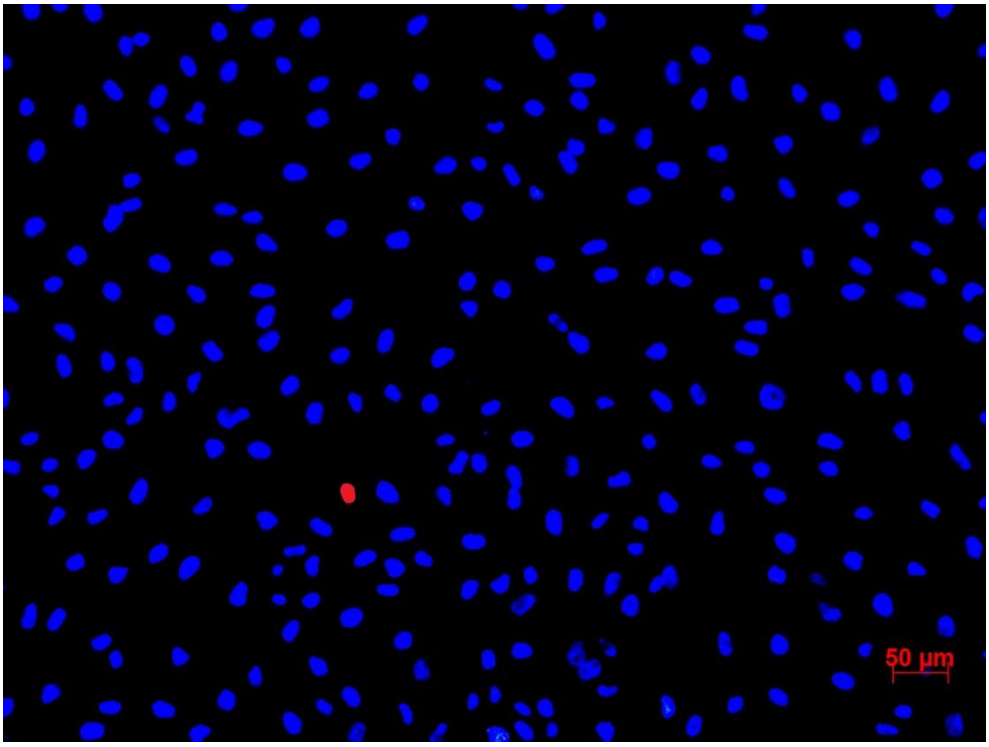

Figure S7. *Fluorescence microscopy image of MG63 cells incubated for 24 h on the non-treated sample (nuclei of viable cells are blue, while nuclei of dead cells are red).*

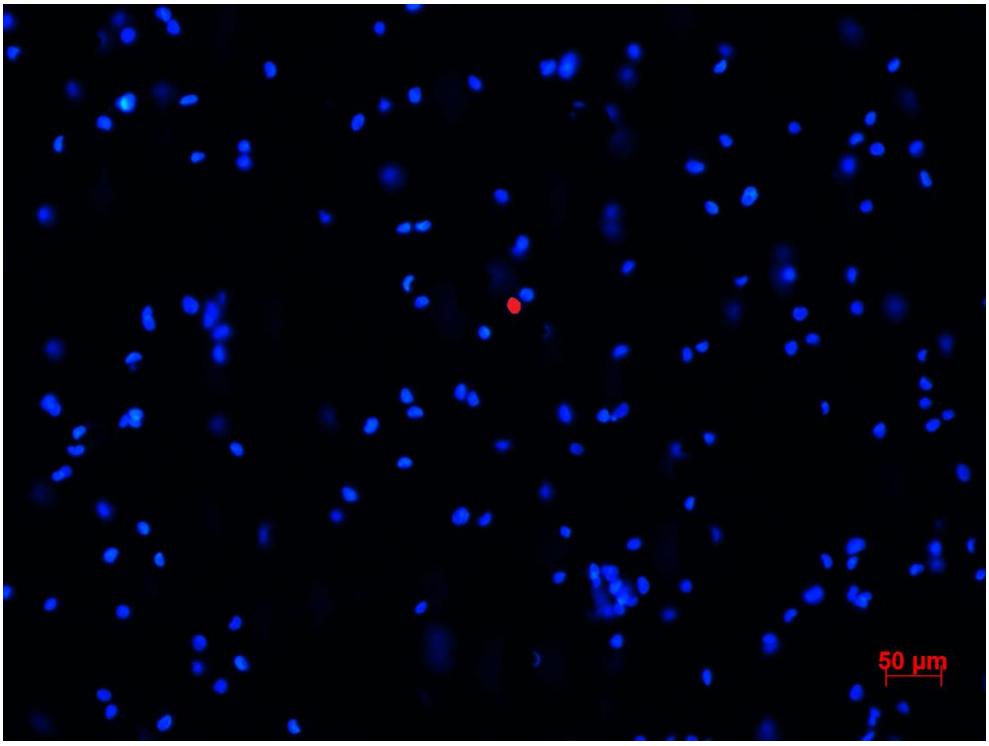

Figure S8. *Fluorescence microscopy image of MG63 cells incubated for 24 h on the laser-textured sample (nuclei of viable cells are blue, while nuclei of dead cells are red).*

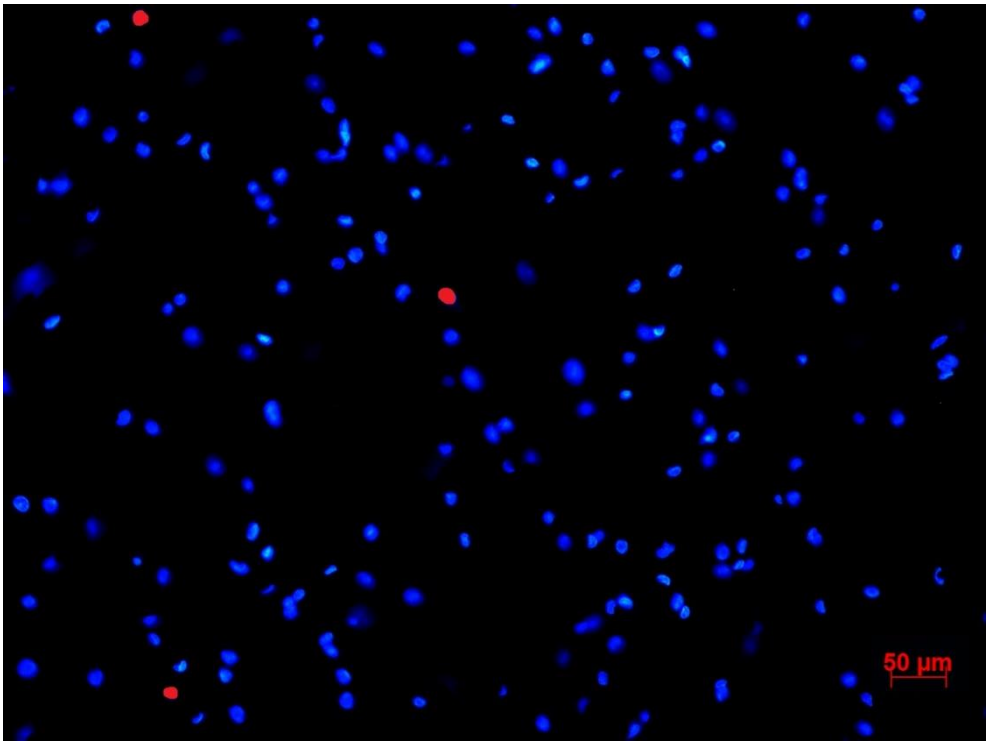

Figure S9. *Fluorescence microscopy image of MG63 cells incubated for 24 h on the laser-textured sample (nuclei of viable cells are blue, while nuclei of dead cells are red).*

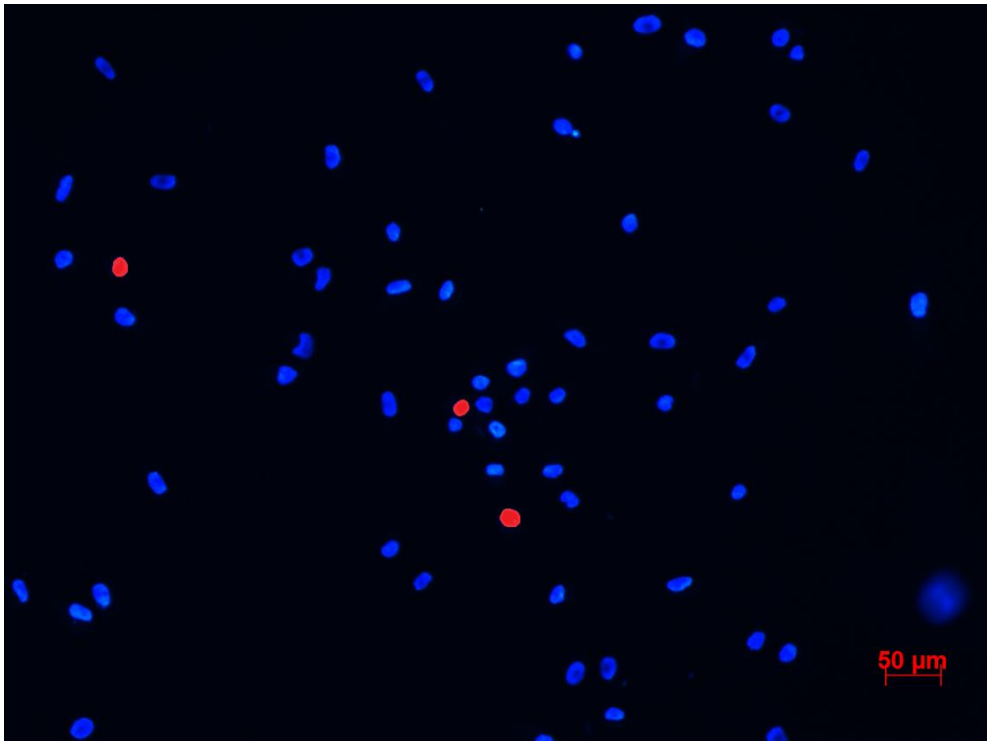

Figure S10. *Fluorescence microscopy image of MG63 cells incubated for 24 h on the glass sample (nuclei of viable cells are blue, while nuclei of dead cells are red).*

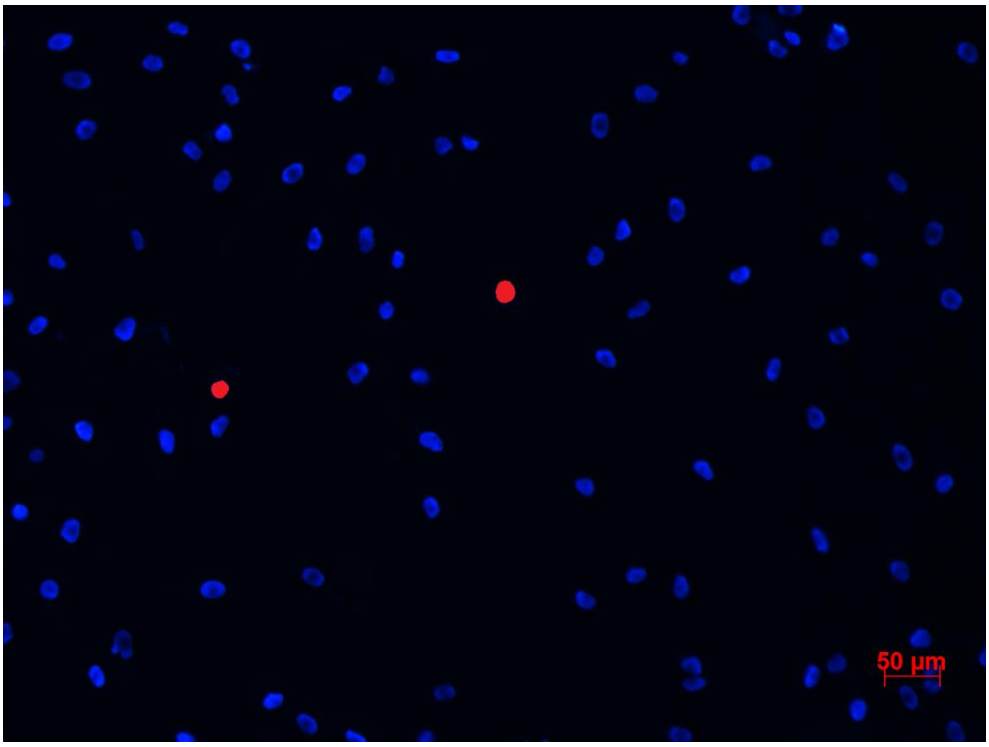

Figure S11. *Fluorescence microscopy image of MG63 cells incubated for 24 h on the glass sample (nuclei of viable cells are blue, while nuclei of dead cells are red).*

S4 SEM of cell adhesion pattern and cell gross morphology

Fluorescence microscopy imaging was followed by SEM observations of the attachment pattern and morphology of MG63 cells on the non-treated and laser-textured surfaces and compared to the control glass surface. From the tested samples, we selected additional images of the most representative cell adhesion pattern and morphology. MG63 cells on the non-treated sample exhibited random orientation (Figure S12) and the majority of cells were polygonal, highly elongated, and flattened (Figure S13). Cell tubular interconnections known as tunnelling nanotubes (TNT) were observed connecting membranes of neighbouring cells (Figure S14). Similar results, random orientation, firmly attaching cells occupying big surface area were observed on control glass surface (Figure S15). Shape of cells and cell surface characteristics are also similar on both surfaces (Figure S16 and Figure S17).

On the other hand, the attachment pattern on the laser-textured samples depend on the laser-textured morphology. Cells are aligned and attached mostly on the groves and the morphology of cells is different. The majority of the cells is round-shaped with smaller footprint, shorter filamentous protrusions (filopodia) and anchoring points (Figure S18), and abundance of extracellular vesicles (Figure S19). This indicates less favourable surface for cell adhesion process and more stress for cells.

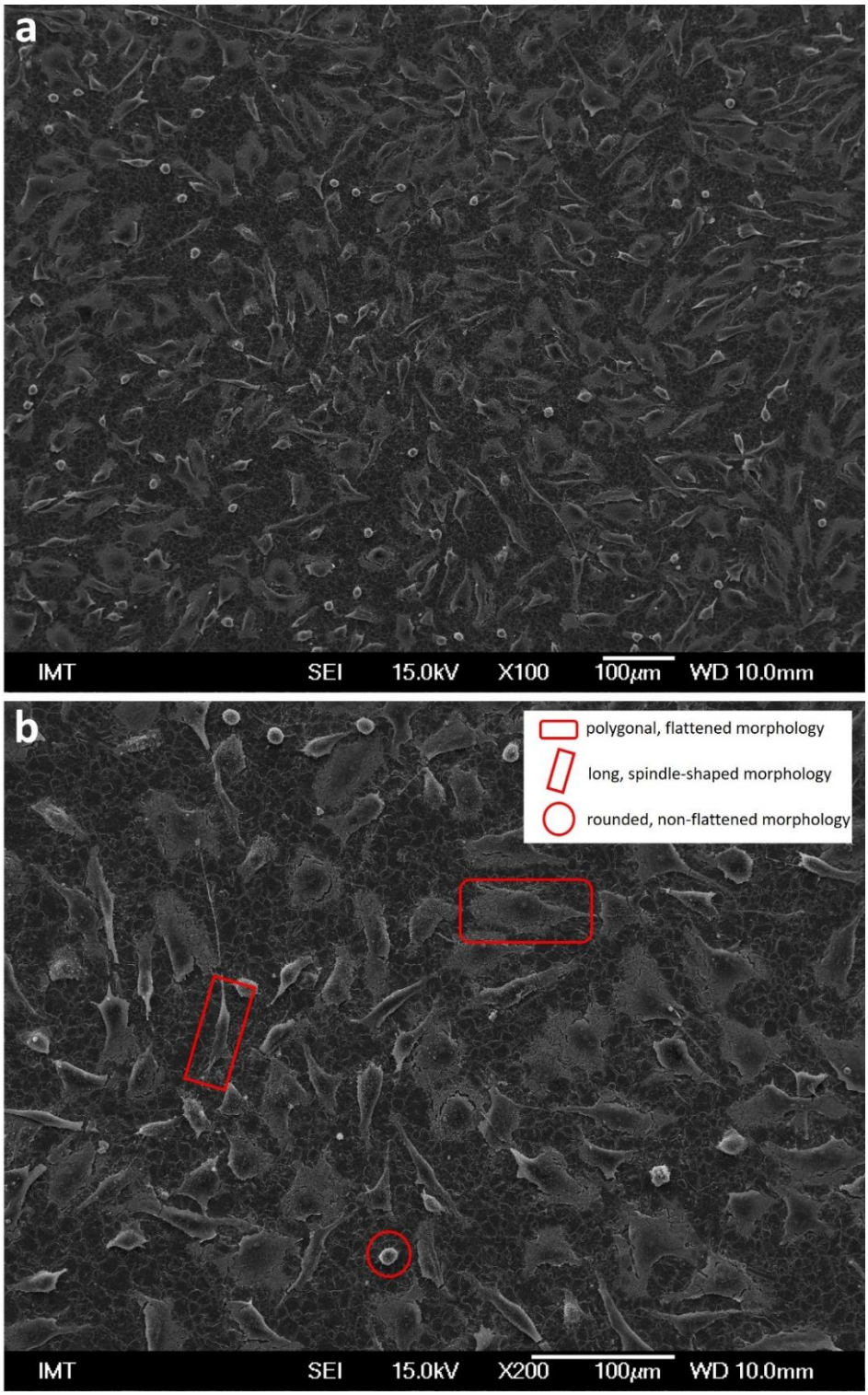

Figure S12. *SEM images of the MG63-cell distribution and shapes on the non-treated sample at two magnifications.*

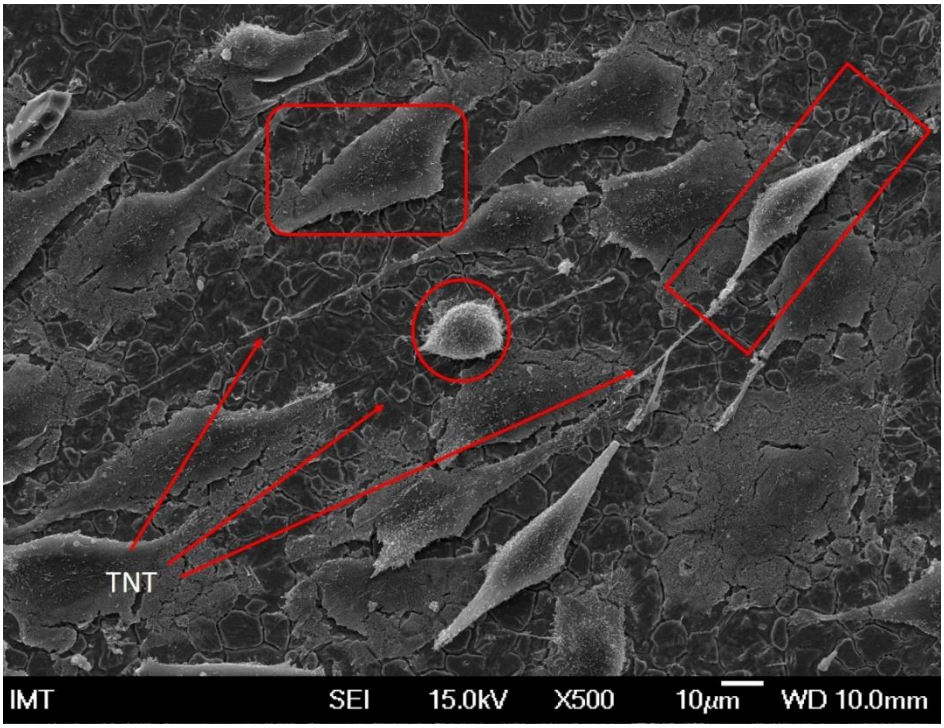

Figure S13. *SEM image of the MG63-cell morphology on the non-treated sample.*

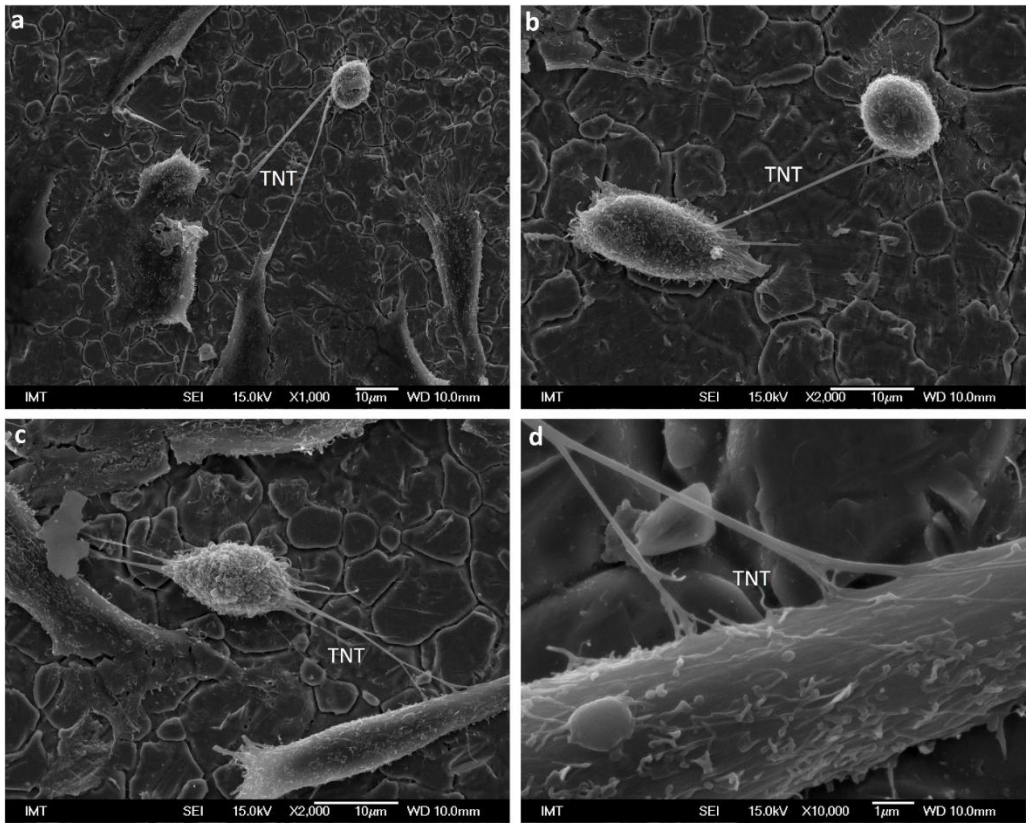

Figure S14. *SEM images of the MG63-cell morphology on the non-treated sample.*

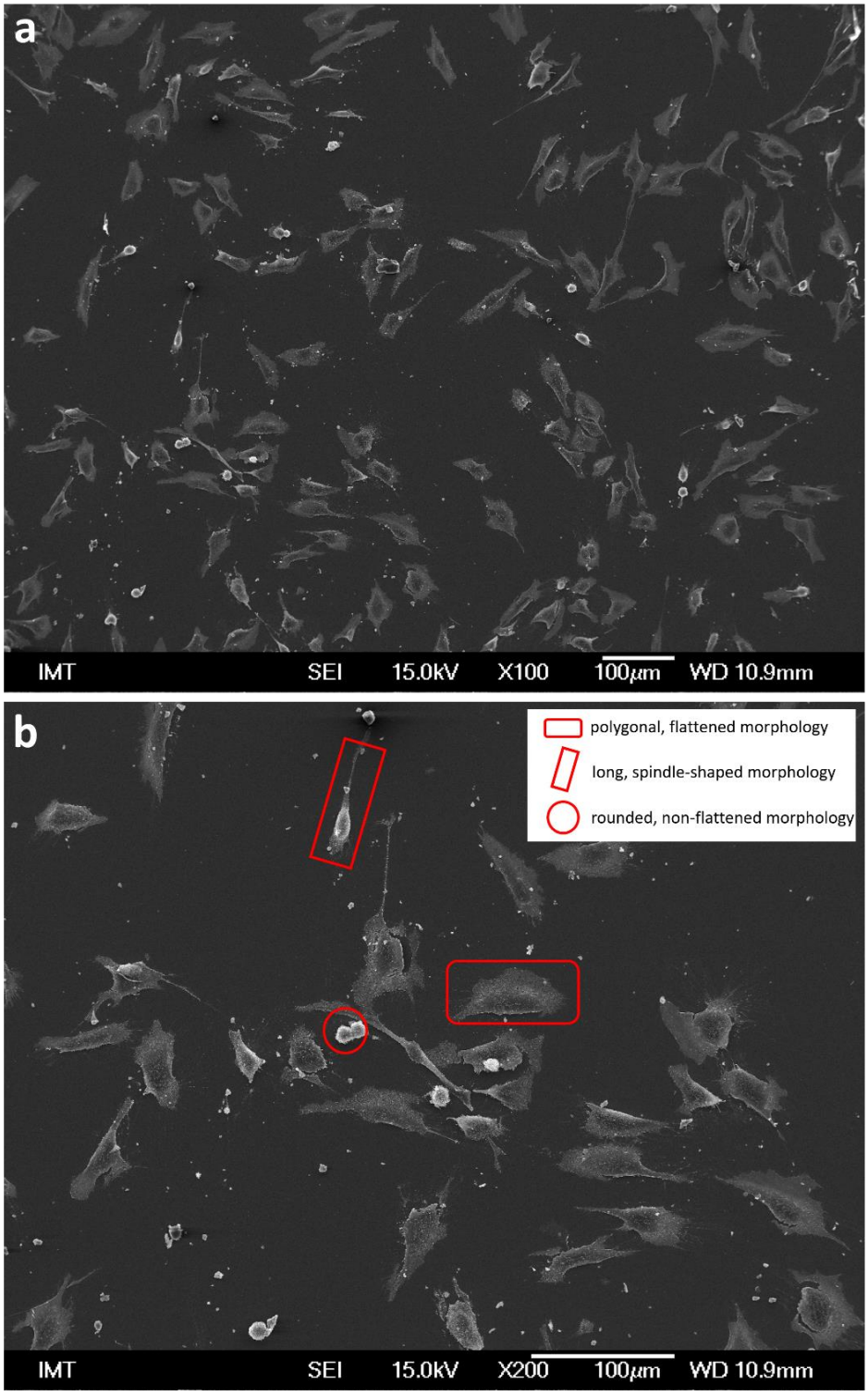

Figure S15. *SEM images of the MG63-cell distribution and shapes on the glass sample at two magnifications.*

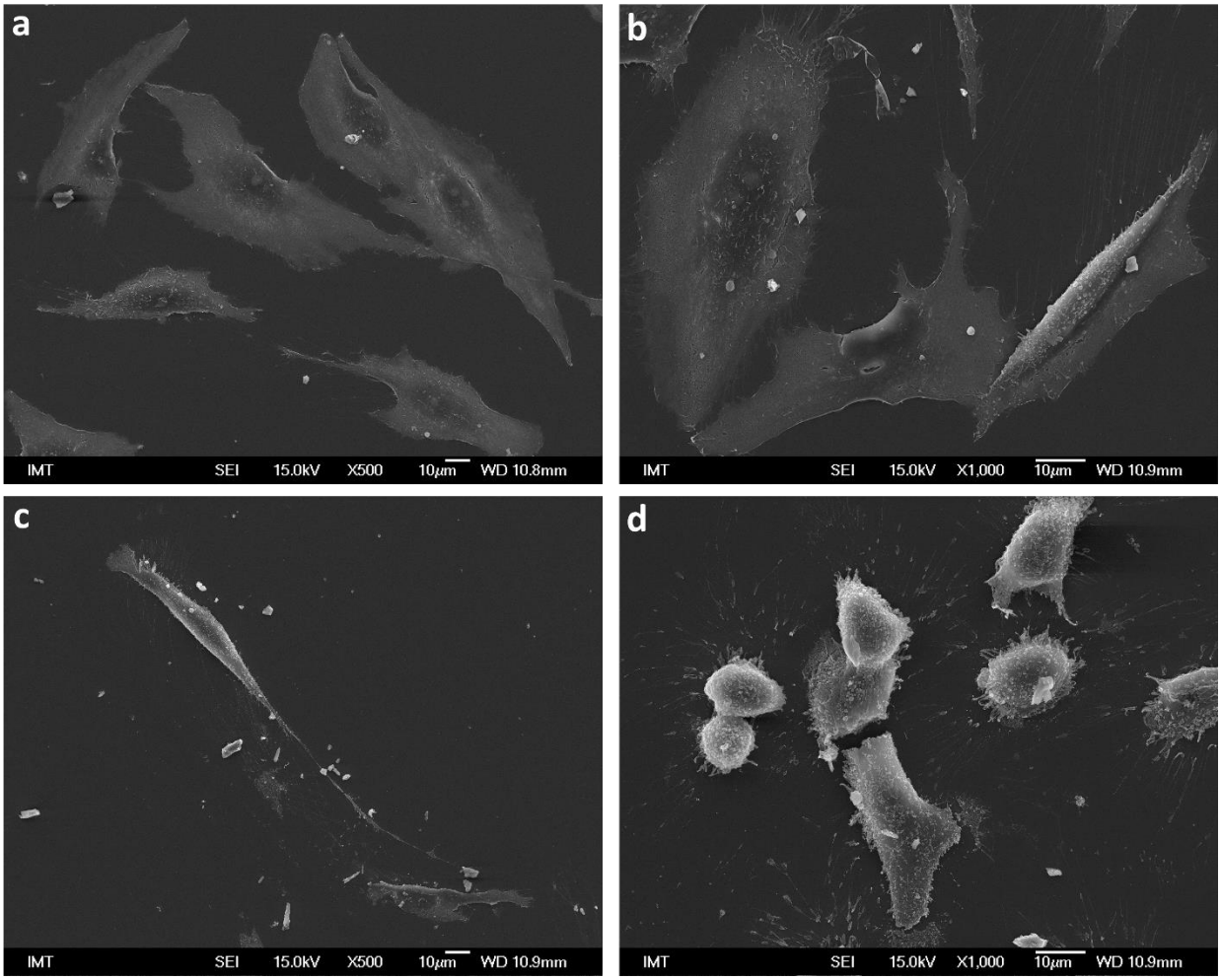

Figure S16. *SEM images of the different MG63-cell shapes on the glass sample at different magnifications.*

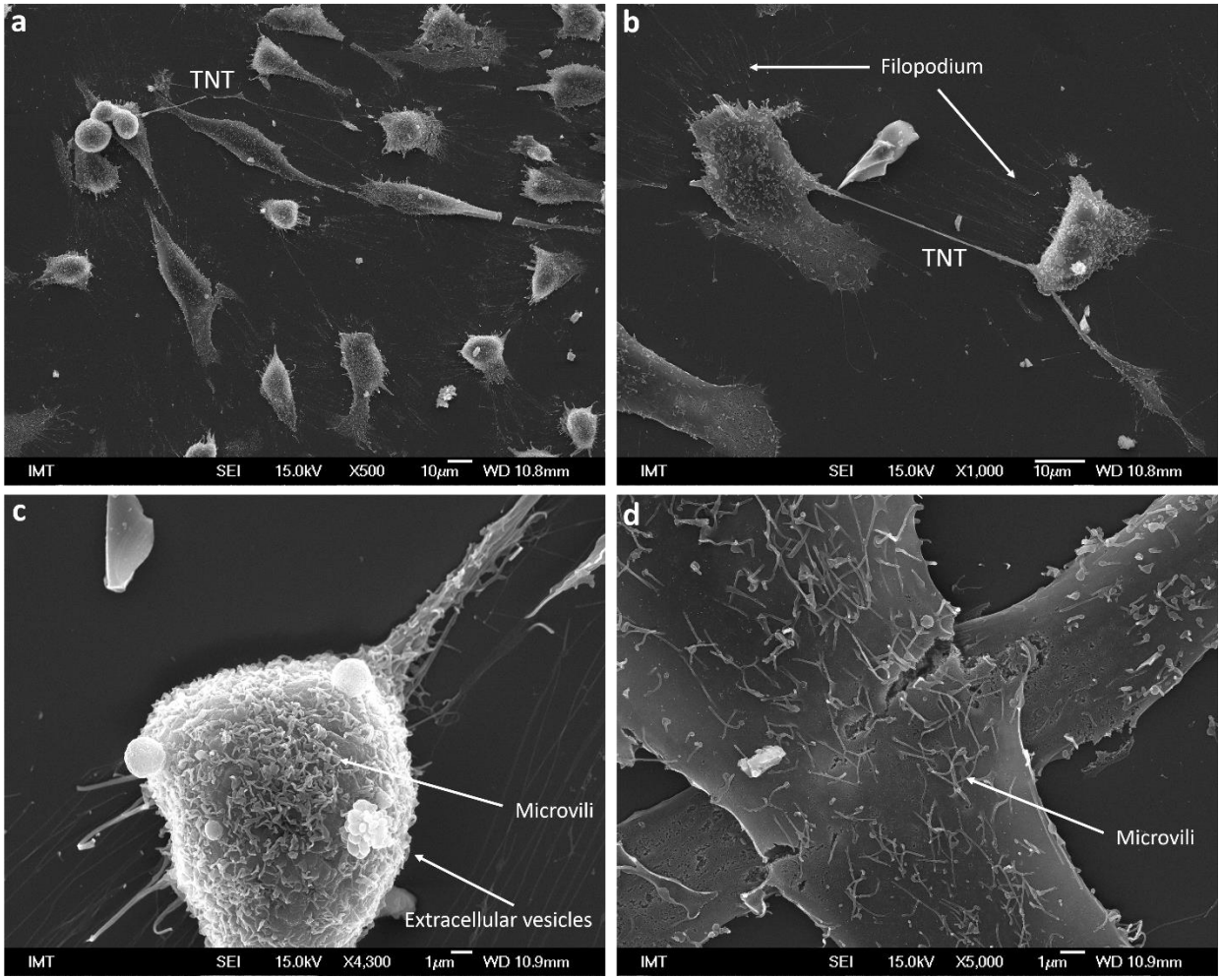

Figure S17. *SEM images of the MG63-cell morphology on the glass sample at different magnifications.*

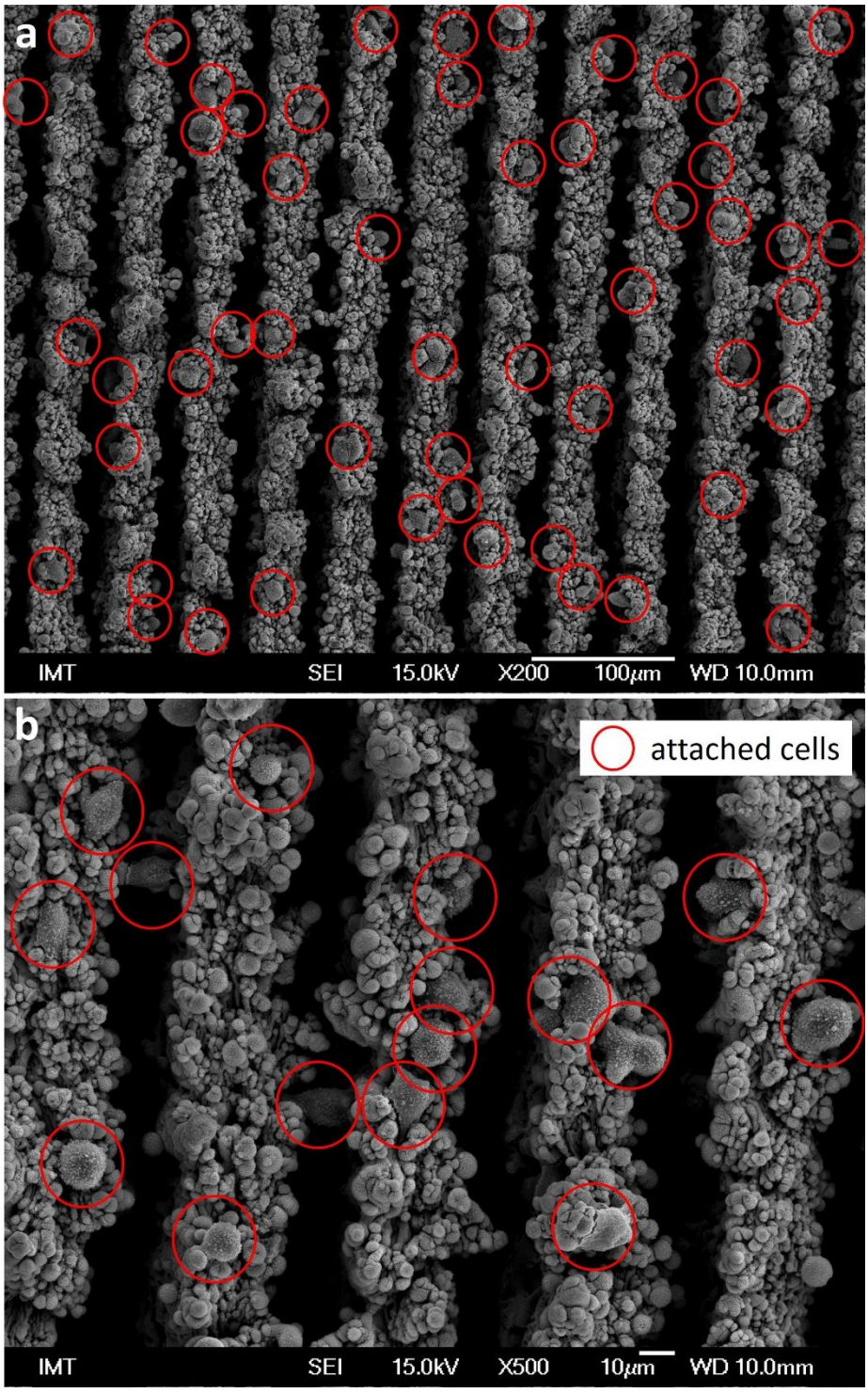

Figure S18. *SEM images of the MG63-cell distribution on the laser-textured sample at two magnifications.*

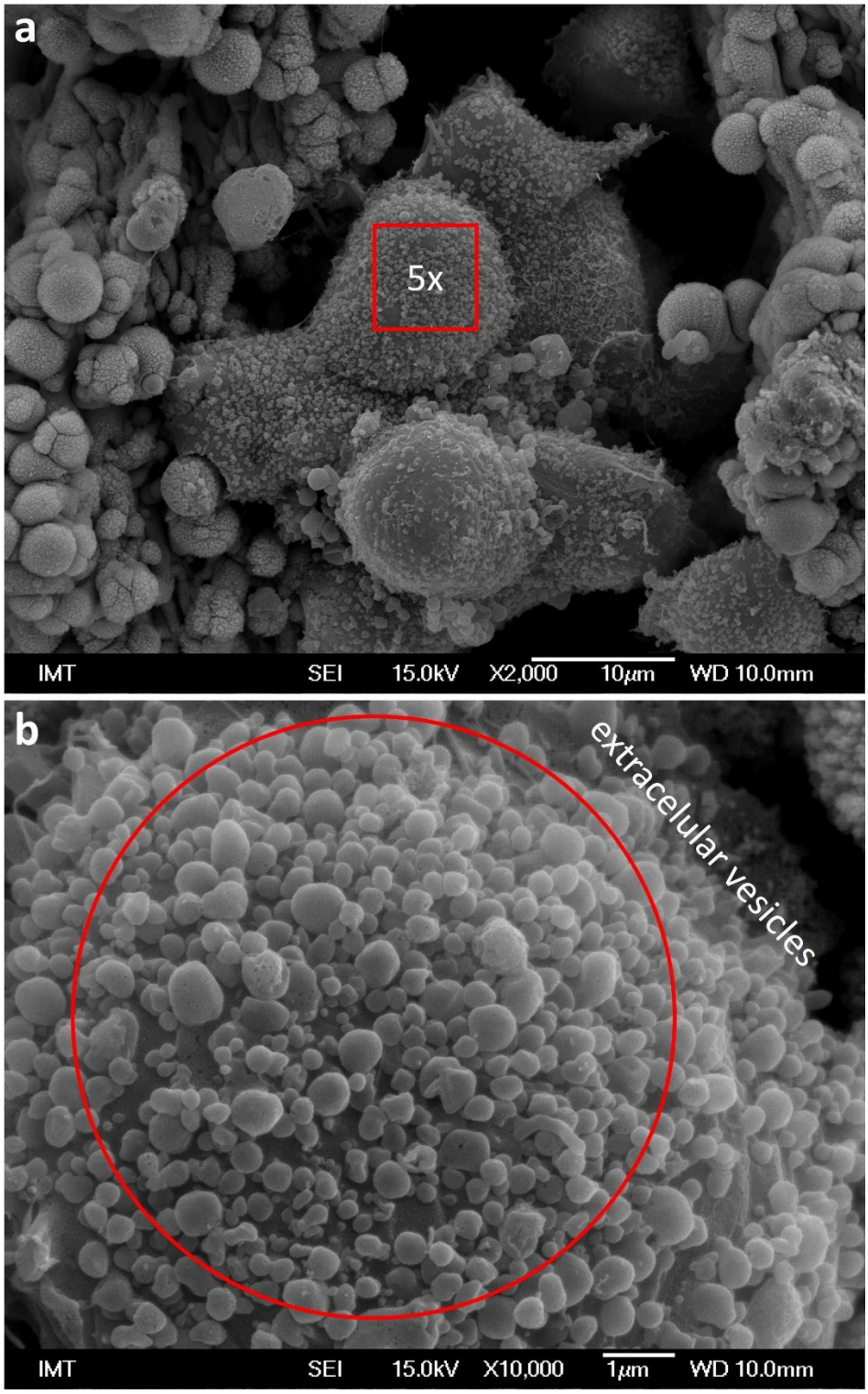

Figure S19. *SEM images of the MG63-cell morphology on the laser-textured sample. Cells are more round shaped and covered with extracellular vesicles.*

S5 References

[S1] R.J. Crawford, H.K. Webb, V.K. Truong, J. Hasan, E.P. Ivanova, Surface topographical factors influencing bacterial attachment, Adv. Colloid Interface Sci. 179–182 (2012) 142–149. doi:https://doi.org/10.1016/j.cis.2012.06.015.